AD-A090 854 PITTSBURGH UNIV PA DEPT OF METALLURGICAL AND MATERI--ETC F/G 11/6
OXIDATION AND OXIDE DISPERSION STRENGTHENING OF COPPER-TITANIUM--ETC(U)
OCT 78 G H MEIER N00014-75-C-0747
UNCLASSIFIED SETEC-MME-78-170 NL

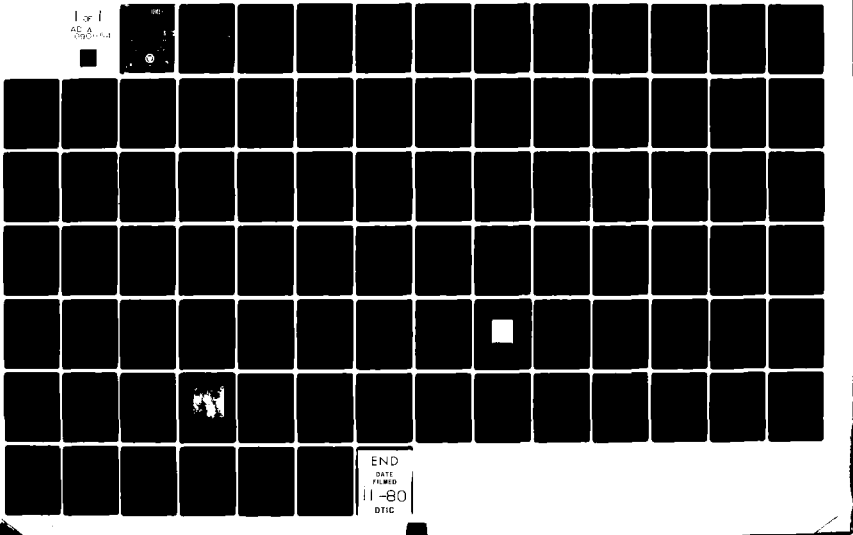

END
DATE FILMED
11-80
DTIC

LEVEL II

METALLURGICAL AND MATERIALS ENGINEERING

University of Pittsburgh
Pittsburgh, Pennsylvania 15261

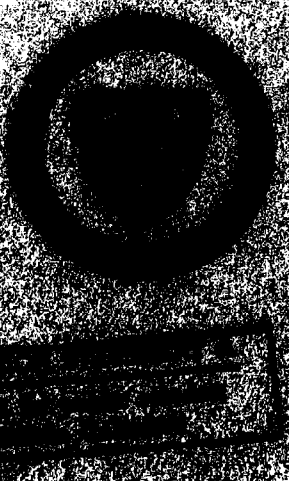

(14) SETEC-MME-78-170

LEVEL II

(1)

(13)

(9) Final Report

(6) Oxidation and Oxide Dispersion Strengthening of Copper-Titanium and Other Alloys

(11) Oct 78

Submitted to

Metallurgy Program
Office of Naval Research
Arlington, Virginia 22217

Contract No N0001475C0747

(13) N00014-75-C-0747

by

(10) Gerald H. Meier
Department of Metallurgical and Materials Engineering
University of Pittsburgh
Pittsburgh, Pennsylvania 15261

October, 1978

SECURITY CLASSIFICATION OF THIS PAGE *(When Data Entered)*

REPORT DOCUMENTATION PAGE

READ INSTRUCTIONS BEFORE COMPLETING FORM

1. REPORT NUMBER	2. GOVT ACCESSION NO. AD-A090 854
3. RECIPIENT'S CATALOG NUMBER	
4. TITLE *(and Subtitle)* Oxidation and Oxide Dispersion Strengthening of Copper-Titanium and Other Alloys	5. TYPE OF REPORT & PERIOD COVERED Final Report
	6. PERFORMING ORG. REPORT NUMBER SETEC-MME-78-170
7. AUTHOR(s) G. H. Meier	8. CONTRACT OR GRANT NUMBER(s) N0001475C0747-ONR
9. PERFORMING ORGANIZATION NAME AND ADDRESS Department of Metallurgical and Materials Engineering, University of Pittsburgh Pittsburgh, Pennsylvania 15261	10. PROGRAM ELEMENT, PROJECT, TASK AREA & WORK UNIT NUMBERS
11. CONTROLLING OFFICE NAME AND ADDRESS Metallurgy Program Office of Naval Research Arlington, VA 22217	12. REPORT DATE October 1978
	13. NUMBER OF PAGES
14. MONITORING AGENCY NAME & ADDRESS *(if different from Controlling Office)*	15. SECURITY CLASS. *(of this report)*
	15a. DECLASSIFICATION/DOWNGRADING SCHEDULE

16. DISTRIBUTION STATEMENT *(of this Report)*

DISTRIBUTION STATEMENT A
Approved for public release;
Distribution Unlimited

17. DISTRIBUTION STATEMENT *(of the abstract entered in Block 20, if different from Report)*

18. SUPPLEMENTARY NOTES

19. KEY WORDS *(Continue on reverse side if necessary and identify by block number)*

Cu alloys, Co alloys, internal oxidation, dispersion hardening, precipitation hardening, coarsening.

20. ABSTRACT *(Continue on reverse side if necessary and identify by block number)*

The kinetics of internal oxidation of dilute Cu-Ti alloys have been studied as a function of specimen geometry, temperature and Ti concentration. Rate equations based on the quasi-steady state approximation have been shown to describe the internal oxidation of both cylinders and spheres. Similar studies on planar Co-Ti alloys have shown multiple internal zones. Rate equations have been formulated for this case and shown to agree with experiments. The above measurements have provided

DD FORM 1 JAN 73 1473 EDITION OF 1 NOV 65 IS OBSOLETE
S/N 0102-014-6601 |

SECURITY CLASSIFICATION OF THIS PAGE *(When Data Entered)*

data for the oxygen permeabilities in both Cu and Co.

The particle size, crystal structure, and morphology of internal Ti oxides in Cu have been carefully investigated and the elevated temperature coarsening of TiO_2 particles has been studied. The coarsening kinetics were found to be diffusion controlled but the rate of coarsening of TiO_2 is much slower than for other oxides (e.g. SiO_2) in Cu.

The TiO_2 dispersion effectively increases the yield strength of Cu-titania alloys by a factor of five to ten over that of pure copper. Good correlation can be made between the yield strengths and the Orowan mechanism for dispersion strengthening. Alloys with Ti concentrations of 1 wt. pct or less are ductile (15 - 30% elongation). The combined mechanical properties (strengths and ductilities) of polycrystalline Cu-TiO_2 alloys are comparable to the best values yet reported for dispersion strengthened copper. The combined effects of a TiO_2 dispersion and Cr precipitates on the mechanical properties of Cu indicate a method for obtaining outstanding mechanical properties in Cu alloy systems.

Table of Contents

Internal Oxidation and Oxide Dispersion Strengthening of Cu and Co Alloys

by

G. H. Meier

I. Kinetics of Internal Oxidation

Internal oxidation has been the subject of numerous investigations during the past decade and several review articles have been published.[1-3] This process is of interest for a number of reasons. Firstly, its occurrence during alloy oxidation may be detrimental in that internal oxidation can prevent the formation of a protective external scale.[4] In some cases, however, internal oxidation has beneficial effects, for example, by improving the adherence of certain external scales.[5] Secondly, internal oxidation provides a method of introducing second phase particles into an alloy which can markedly affect the mechanical,[6,7] magnetic,[8,9] and other properties of the alloy. Finally, internal oxidation kinetic measurements have been used to estimate the solubility-diffusivity product for oxygen in solid copper,[10-15] silver,[13] iron,[16,17] and nickel.[18]

The kinetics of internal oxidation in simple cases for planar specimens and alloys in which only one oxide forms have been extensively studied. Often, however, more complicated specimen geometries are of interest, e.g. in the internal oxidation of wires or powders and in many alloy systems more than one oxide forms during internal oxidation. In the present investigation the effect of specimen geometry has been investigated in the internal oxidation of cylindrical and spherical specimens of Cu-Ti alloys and the formation of multiple zones of internal oxidation have been studied in dilute Co-Ti alloys.

A. Internal Oxidation of Cu-Ti Cylinders and Spheres

1. Background

Rate equations for the internal oxidation of flat specimens have been derived by several authors,[11,12,19,20] assuming diffusion control, for the case of internal oxidation in the absence of external scale formation. Wagner[20] rigorously solved the diffusion problem and presents equations from which the penetration of the internal oxidation front may be calculated as a function of time. For the special case of $D_B/D_O << N_O^{(s)}/N_B^{(o)} << 1$; where D_B and D_O are the diffusivities of solute and oxygen respectively, $N_O^{(s)}$ is the atom fraction of dissolved oxygen at the specimen surface, and $N_B^{(o)}$ is the atom fraction of solute in the alloy; Wagner's equation for the front penetration (ξ) reduces to

$$\xi = \left[\frac{2N_O^{(s)} D_O t}{\nu N_B^{(s)}} \right]^{\frac{1}{2}} \qquad (1)$$

where t is the oxidation time and ν is the stoichiometric coefficient in BO_ν. This same equation is obtained more simply by neglecting solute diffusion and assuming the dissolved oxygen concentration gradient is essentially that which would exist for a stationary front. This quasi-steady state approximation has been used by Swisher and Fuchs[21] to derive an expression for the rate of penetration of the internal oxidation zone into cylindrical and spherical specimens, cases which have not been treated rigorously. The following expression may be used to describe the rate of internal oxidation of the cylindrical copper-titanium specimens used in the present investigation.

$$Y \equiv \frac{(r_1)^2}{2} - (r_2)^2 \left[\ln \frac{r_1}{r_2} + \frac{1}{2} \right] = \frac{N_O^{(s)} D_O}{\nu N_{Ti}^{(o)}} t \qquad (2)$$

where

r_1 is the outer radius of the specimen, cm.

r_2 is the radius of the unoxidized alloy core, cm.

The corresponding expression for spherical specimens is

$$X \equiv \frac{r_1^2}{3} - r_3^2 + \frac{2}{3}\frac{(r_3)^3}{r_1} = \frac{N_O^{(s)} D_O}{\nu N_{Ti}^{(o)}} t \qquad (3)$$

where

r_3 is the radius of the unoxidized spherical core, cm.

The quantities Y and X will be referred to as the penetration parameters. Experimental verifications of the validity of the quasi-steady state approximation for the internal oxidation of cylinders have been reported for Cu-Cr[21] and Cu-Zr[22] alloys by Swisher and Fuchs and for Cu-Ti alloys in previously published results of the present investigation.[23,24] There are no published investigations of the internal oxidation of spheres.

2. Experimental Procedure

The procedure used in studying the internal oxidation of Cu-Ti cylinders has been published previously.[23,24] A similar procedure was used for the oxidation of spheres and will be briefly described. Cylindrical sections approximately one cm in length were cut from a 6 mm diamter, as-swaged, Cu-0.29 wt pct Ti rod. Hemispherical caps were then machined onto one end of each rod and the specimens were solution annealed at 850°C for 48 hrs in evacuated, Ti-gettered Vycor capsules and quenched in ice water. The specimen surfaces were then prepared by electropolishing in a solution of 750 ml acetic acid, 150 gm chromium trioxide and 30 ml distilled water using a hollow copper cathode in the same shape as the specimen. Immediately after electropolishing the specimens were packed in a powder mixture of 30 vol pct Cu_2O, 20 vol pct Cu and 50 vol pct Al_2O_3 and encapsulated under vacuum in Vycor. The specimens were oxidized by heating the capsules in a Lindberg Hevi-Duty tube furnace at temperatures of 700, 750, 800, 850, and 900°C for times up to 200 hrs. The specimens were sectioned as shown in Figure 1. From section BB', which is taken at random through the spherical portion of the specimen,

$$r_1^2 = l_1^2 + h^2 \tag{4}$$

and

$$r_3^2 = l_2^2 + h^2 \tag{5}$$

so that r_1 and r_3 may be obtained by measurement of l_1, l_2, and h on a polished and etched section such as AA'. Similarly r_1 and r_2 for the cylindrical gemoetry may be obtained directly from a section such as BB'. Figure 2 shows the appearance of the internal oxidation zone after etching.

3. Results and Discussion

Figure 3 shows a typical plot of penetration of the internal oxidation zone (r_1-r_2 or r_1-r_3) vs square root of time for the cylindrical and spherical portions of the same specimen. The curvature of the plots is predicted by Eqns. 2 and 3 whereas a straight line would be expected for a planar specimen. Figure 4 shows the same data plotted as penetration parameter (X or Y) vs time. Assuming ν=2 for TiO_2 precipitates[24] these two plots should superpose with slope equal to $\frac{N_O^{(s)} D_O}{N_{Ti}^{(o)}}$ as seen from Eqns. 2 and 3. There is some scatter of data points about each line but the least square lines are seen to nearly superpose giving calculated values of $N_O^{(s)} D_O$ in close agreement (see Table 1). The equations best fitting the data of Table 1 are

$$N_O^{(s)} D_O = (3.37 \begin{smallmatrix} + 10.0 \\ - 3.5 \end{smallmatrix}) \exp\left(-\frac{63760 \pm 2930 \text{ cal/mole}}{RT}\right) \tag{6}$$

for cylinders and

$$N_O^{(s)} D_O = (5.17 \begin{smallmatrix} + 26.5 \\ - 4.32 \end{smallmatrix}) \exp\left(-\frac{64570 \pm 3850 \text{ cal/mole}}{RT}\right) \tag{7}$$

for spheres. The results indicate that the equations derived from the quasi-steady state approximation can adequately describe the kinetics of internal oxidation of both cylinders and spheres.

B. Internal Oxidation of Co-Ti Alloys

The studies of the internal oxidation of dilute Cu-Ti alloys have indicated the presence of several Ti oxides in the precipitates formed in the Cu-matrix.[24,25] While this is not surprising on thermodynamic grounds, the structure of the oxides formed at various distances below the specimen surface as the internal oxidation front moves through is important for understanding the details of the internal oxidation process. Unfortunately, from this standpoint, the Ti oxide particles formed in Cu are extremely small[24] and make a detailed structural analysis difficult. Therefore, a study of internal oxidation in the Co-Ti system was undertaken since one would expect larger oxide particles to form in a Co rather than Cu matrix. Furthermore, since no detailed studies of internal oxidation in Co base alloys have been reported a study of the kinetics of internal oxidation of Co-Ti alloys offered the opportunity to determine the permeability of oxygen in Co.

The formation of two or more oxides by internal oxidation has been observed in several systems but the phenomenon has not been analyzed in most cases. The work of Levy and Niessen[26] on the internal oxidation of Ag-Mn alloys indicates the formation of MnO at 750°C but suggests the formation of more than one oxide at 910°C. The formation of Mn_2O_3 and Mn_3O_4, as well as MnO, was reported for internally oxidized Cu-Mn alloys.[27] Both SnO and SnO_2 are formed in Ag-Sn alloys[28] and both Fe_3O_4 and $CuFeO_2$ are formed in Cu-Fe alloys oxidized at high oxygen pressures.[29]

The most detailed study of the formation of multiple oxides by internal oxidation is the work of Kapteijn[30] on the internal oxidation of Ag-Cu alloys. It was observed that the oxide particles near the internal oxidation front were Cu_2O which was further oxidized to CuO as the local oxygen activity was increased by the inward diffusion of oxygen from the

specimen surface. An intermediate zone containing both Cu_2O and CuO was observed between the Cu_2O and CuO regions. The oxidation kinetics were analyzed using a model due to Meijering[31] which is reviewed in Appendix A. In short this model considers the formation of a lower oxide BO_{n_1} at a planar internal oxidation front which lies at a distance ξ below the specimen surface and the further oxidation of BO_{n_1} to a higher oxide BO_{n_2} (or a double oxide) at a second front at a distance η below the specimen surface. The motion of both fronts is assumed to be controlled by the inward diffusion of oxygen so that the ratio

$$f = \eta/\xi \tag{8}$$

is a constant independent of time and concentration of oxidizable solute. The penetration of the internal oxidation zone is expressed by

$$\xi^2 = \frac{2N_O^{(s)}D_O}{n_{eff}N_B^{(o)}}\, t \tag{9}$$

where $N_B^{(o)}$ = mole fraction of solute B initially in the alloy,

$N_O^{(s)}$ = solubility of oxygen in the matrix A,

D_O = diffusivity of oxygen in A (cm^2/sec),

t = time of oxidation (sec),

and n_{eff} = an effective stoichiometric coefficient given by

$$n_{eff} = \frac{n_1(1 - f)}{m} \tag{10}$$

where $m = (p_{O_2}^{(\eta)}/p_{O_2}^{(o)})^{\frac{1}{2}}$, the square root of the ratio of the local oxygen pressure at the intermediate front (η) to that at the specimen surface.

Eqn. (9) may be compared with the analogous equation describing internal oxidation in which a single oxide (BO_n) is formed

$$\xi^2 = \frac{2N_O^{(s)}D_O}{n\,N_B^{(o)}}\, t \tag{11}$$

Kapteijn's results obeyed Eqn. (9) reasonably well and f was observed to be independent of oxidation time. No investigation was made of the effect of varying solute concentration. It should be noted that, for matrix metals for which $N_O^{(s)}D_O$ is unknown, measurements of ξ as a function of t for a known $N_B^{(o)}$ will allow the use of Eqn. (9) for the calculation of $N_O^{(s)}D_O$ providing n_{eff} can be calculated.

Studies of internal oxidation in Co-base alloys are quite rare in the literature. Nolan and Grundy[34] studied the oxide morphologies produced by internal oxidation of Co-Si alloys containing less than 2 wt% Si. The SiO_2 particles were observed to be spherical near the surface of the alloy and became larger with increased depth below the specimen surface. At still greater depth below the surface the oxide particles became elongated in the direction perpendicular to the specimen surface and eventually grew as long filaments. This change in morphology with increased depth below the specimen surface may be understood from the fact that the internal oxidation front is moving slower the deeper it penetrates which allows more time for the diffusion of Si to a growing particle before the nucleation of another particle. This results in an increased particle size with increased depth and eventually allows the growth of a particle to keep pace with the internal oxidation front producing filamentary particles. The increase in particle size with depth for spherical particles has been analyzed theoretically by Böhm and Kahlweit.[33] The kinetics of internal oxidation of dilute Co-Si alloys have been examined briefly by Grundy and Nolan.[34]

1. Experimental Procedure

1.1 Alloy Preparation

Co-Ti alloys with Ti contents ranging from 0.5 to 7.43 wt percent were melted in a tungsten arc furnace under an argon atmosphere and drop cast into a copper mold. The specimen surfaces were prepared by metallographic polishing through 0.05 micron alumina, annealing for 1 hour at 1000°C, water

quenching, and then repolishing with 0.05 micron alumina. Care was taken to insure the surfaces of each specimen were identical.

1.2 Internal Oxidation Procedure

All specimens were oxidized using a "Rhines pack" technique. The specimens were packed in a powder mixture of equal parts by weight Co, Co_3O_4, and Al_2O_3 and sealed in evacuated quartz capsules. The Co and Co_3O_4 powder served to establish the oxygen partial pressure at the dissociation pressure of CoO while the Al_2O_3 served to minimize sintering of the powder to the specimen. Each capsule contained one specimen of each alloy (0.50, 1.01, 3.01, 4.96, and 7.43 wt percent Ti). Oxidation temperatures of 900, 1000, and 1080°C were used with at least four oxidation times being employed for each temperature.

1.3 Optical Microscopy

Oxidized specimens were sectioned perpendicular to the internal oxidation front, and examined optically in the overpolished and unetched condition. These observations revealed two parallel zones of internal oxidation with different oxide colors and morphologies in each. The penetration of both zones was measured using a filar eyepiece calibrated for each magnification used.

1.4 Oxide Structure Determination

Internally oxidized specimens were polished (parallel to the internal oxidation fronts) to various depths and the crystal structure of the oxide particles was investigated using a G.E. XRD-5 diffractometer using Co-K_α radiation. Carbon extraction replicas were also prepared from the polished surfaces and examined in a JEOLCO 120U electron microscope operating at an accelerating voltage of 120 KV.

2. Results and Discussion

The results of this portion of the investigation have been published previously[35,36] and will be reviewed briefly here.

2.1 Oxide Morphology and Crystal Structure

The morphology of the internal oxide particles was observed to change markedly with Ti content, oxidation temperature, and depth below the specimen surface. Figure 5 shows the oxide morphology in a Co-0.5 wt percent Ti alloy internally oxidized for 528 hours at 900°C. The penetration of the internal oxidation zone is indicated at $x = \xi$. Also, although not evident on a black-white micrograph, the color of the oxide particles changed markedly at an intermediate front indicated at $x = \eta$. The particles at $x<\eta$ exhibited a gray color while those at $x>\eta$ were yellow. X-ray and electron diffraction indicates this color change is associated with a change in crystal structure of the oxide particles. A third structure is indicated by x-ray diffraction for penetrations $x>\xi$ although these particles are not apparent in the optical micrographs. The comparison of the results from x-ray determinations of the structure of the oxides and those from optical microscopy presented in Figure 6 appear confusing since the boundaries of the zones do not coincide for the two techniques. However, this can be understood if the internal oxidation process is assumed to occur in the following manner. The oxide nucleates at the reaction front as δ-TiO. However, since there is very little difference in stability between TiO and TiO_2 the TiO zone is never observed optically. As the oxygen activity continues to increase the TiO_2 reacts with Co and O to form $CoTiO_3$. The reason that a zone containing only TiO is observed with x-rays is, presumably, that the volume fraction of the TiO_2 growing around the TiO particles is not sufficient to give a measurable x-ray intensity. Closer to the specimen surface the volume fractions of both TiO and TiO_2 are sufficient to produce measurable x-ray intensities. Still closer to the

surface all of the TiO has been reacted to TiO_2 and x-rays indicate only TiO_2 present. The intermediate front at $x = \eta$, observed optically, marks the deepest position in the specimen where the TiO_2 has started to react with Co and O to form $CoTiO_3$. Again, however, since the $CoTiO_3$ forms as a shell around the TiO_2 requiring diffusion through this layer for further growth, the volume fraction of $CoTiO_3$ is not sufficient for x-ray observation. Nearer the specimen surface a significant volume fraction of both $CoTiO_3$ and TiO_2 are present and in the region nearest the surface only $CoTiO_3$ is present.

2.2 Kinetics of Internal Oxidation

The penetration of the internal oxidation front (ξ) and the intermediate front (η) were measured for each alloy and each temperature of oxidation. Figure 7 shows ξ plotted versus the square root of oxidation time for a temperature of 1000°C. It is observed that the front penetration varies linearly with $t^{\frac{1}{2}}$ for each of the alloys and temperatures in question. It was also observed that η increases as $t^{\frac{1}{2}}$ as well. Table 2 shows the ratio $f = \eta/\xi$ for three alloys 0.50 wt percent Ti ($N_{Ti} = 0.0061$), 1.01 wt percent Ti ($N_{Ti} = 0.0124$) and 3.01 wt percent Ti ($N_{Ti} = 0.0370$). The ratio is independent of time (since both fronts penetrations move as $t^{\frac{1}{2}}$) but increases with both increased Ti content and increased temperature of oxidation.

The linearity of plots of internal oxidation zone penetration versus square root of time (e.g. Figure 7) indicates the internal oxidation kinetics should be amenable to description by an expression such as Eqn. (9) which may then be used to calculate the oxygen permeability in Co. The problem is the calculation of the effective stoichiometric coefficient, n_{eff} since three oxides are formed in Co-Ti alloys. To make this calculation possible the inner zone ($\eta \leq x \leq \xi$) was taken to contain only TiO_2 ($n_1 = 2$) and the outer zone ($0 < x \leq \eta$) was taken to contain only $CoTiO_3$ ($n_2 = 3$). Table 3 shows the values calculated for n_{eff} calculated from Eqn. (10) and the oxygen permeabilities in Co calculated using Eqn. (9) and the slopes of plots

such as Figure 7. The permeability data for two alloys are plotted in Figures 8 and 9. The oxygen partial pressure at the specimen surface $p_{O_2}^{(o)}$ was taken as the dissociation pressure of CoO[37] and $p_{O_2}^{(n)}$ was taken from the data of Brezny and Muan[38] for the equilibrium

$$TiO_2(s) + Co(s) + \tfrac{1}{2}O_2(g) \leftrightarrow CoTiO_3(s) \qquad (12)$$

The theoretical values of the ratio f calculated from Eqn. (A6), also shown in Table 3, were used in the calculation of $N_O^{(s)}D_O$. It must be noted that the experimental values for f (Table 2) deviate markedly from the theoretical values and exhibit an increase with increasing solute concentration. The difference between the theoretical and experimental values for f is due to uncertainties in the values chosen for n_1 and n_2 and to the fact that the counter-diffusion of Ti was neglected in the derivation of the rate equations in Meijering's analysis. In order to estimate the effects of uncertainties in n_1 and n_2, upper and lower limiting values for $N_O^{(s)}D_O$ were calculated from Eqn. (11) assuming values for n of 3 and 1 respectively. These points are included in Figures 8 and 9 as dashed lines. As can be seen the uncertainties in n affect the magnitude of $N_O^{(s)}D_O$ but not the activation energy which is approximately 50 kcal/mole. Inclusion of the counterdiffusion of Ti in the calculations of $N_O^{(s)}D_O$ requires a reformulation of the rate equations for the case of internal oxidation when two zones are formed.[39] This derivation is presented in Appendix B. The equation necessary for calculation of $N_O^{(s)}D_O$ is

$$N_O^{(s)}D_O = \frac{2N_{Ti}^{(o)}}{m}\,\frac{\xi(\xi-\eta)}{2t}\,\frac{1}{F\left[\frac{\xi}{2(D_{Ti}t)^{\frac{1}{2}}}\right]} \qquad (13)$$

which is Eqn. (B15) written for an inner zone of TiO_2. Values of $N_O^{(s)}D_O$ calculated from Eqn. (13) are tabulated in Table 4 and are included in Figures 8 and 9. It can be seen that values for $N_O^{(s)}D_O$ calculated from Eqns. (9) and (13) agree quite well at 1080°C but deviate somewhat as the oxidation temperature is decreased. It is felt that the values calculated

from Eqn. (13) are the most reliable, even though errors are still introduced due to uncertainties in n_1, since n_2 is eliminated from the calculations and counterdiffusion of Ti is taken into account. The use of the experimental rather than theoretical values for f in calculating n_{eff} would eliminate most of the discrepancy between the $N_O^{(s)}D_O$ values calculated from Eqns. (9) and (13) so that for the Co-Ti system the two analyses are almost equivalent. However, for systems containing a more mobile solute counterdiffusion of solute will be more important and, whenever possible, use of the analysis in Appendix B is preferred.

II. Structure and Morphology of TiO_2 Precipitates in Cu

A. Background

1. Primary Particle Size

The morphology of the particles in an internally oxidized alloy is determined by the competition at the reaction front between the growth of the existing particles and the nucleation of new particles plus any coarsening of the particles which occurs after the front has passed. In general, small particles are favored by factors which result in high nucleation rates. These include high stability of the solute oxide relative to the lowest oxide of the base metal, low interfacial free energy for the particle-matrix interface, and high velocity of the oxidation front. The front velocity is higher for high permeabilities for oxygen in the matrix metal, and small penetrations of the internal oxidation front. Small particles are also favored by factors which result in low growth rates, e.g., low diffusivity for the solute in the matrix metal and low solute contents. Furthermore, small particles are favored by factors which result in low coarsening rates, such as, lower solubility of the oxide particles in the matrix and lower particle-matrix interfacial free energy. Böhm and Kahlweit[33,40] have analyzed the diffusion-controlled growth of spherical BO internal oxide particles in planar specimens. Their analysis predicts that the average particle radius should vary as,

$$r(X) = \left[\frac{3V_{BO}N_B^{(o)}}{4\pi\beta}\right]^{\frac{1}{3}} \frac{X}{N_O^{(s)}} \qquad (14)$$

where, V_{BO} is the molar volume of the oxide, $\frac{cm^3}{mole}$, X is the distance below the specimen surface, cm, β, is a parameter which is independent of $N_O^{(s)}$ (the oxygen solubility in base metal, atom fraction) and X, and is given by,

$$\beta = \left[\frac{1}{N_O^{(s)}} \frac{X}{\Delta X}\right]^3 \qquad (15)$$

where ΔX is the distance covered by the oxidation front between two successive nucleation events. The important predictions of equation (14) are the linear increase of the particle radius with distance below the specimen surface, the decrease in particle radius with increasing oxygen solubility in the matrix, and the increase in particle radius with increasing solute concentration. The equation (14) derived by Böhm and Kahlweit[33] considers only the nucleation and growth of the particles and neglects any changes due to subsequent coarsening or oxidation to a higher oxide. The former of these, coarsening, is of primary significance in determining the stability of an oxide dispersion and will be considered in detail.

2. Coarsening

2.1 Theoretical Considerations

Provided there is some atomic mobility and solubility, a dispersoid of second phase particles will tend to "coarsen" by transfer of matter from small to larger particles. The driving force for this process is derived from the consequent reduction in free energy associated with the particle/matrix interfacial area. The first rigorous quantitative development of the theory of particle coarsening was developed virtually simultaneously by Lifshitz and Slyozov[41] and by Wagner[42] in 1961. Since the development of the coarsening theory, reviews of particle coarsening have been published by Greenwood[43] and Li and Oriani.[44]

The development of the Lifshitz-Wagner theory of particle coarsening is based on the following assumptions:

(1) Particles are of a pure substance and of equilibrium spherical shape.

(2) The particles are dispersed in a fluid matrix and it is assumed that the matrix cannot support stress.

(3) The interparticle spacing is larger than the diameter of the particles.

(4) For longer times of coarsening, the particle size distribution function may be expressed as a product of a pure time function and a function of the radius ratio, r/r^*, where r^* is the radius of the particle which neither grows nor dissolves.

Based on the above assumptions, quantitative equations of coarsening were derived for two different cases where the rate controlling mechanisms are different. The first one is "diffusion-controlled coarsening" where diffusion through the matrix is the slowest step of material transfer and the second one is "reaction controlled coarsening", where the dissolution or deposition of atoms at the particle/matrix interface is the slowest step.

2.1.1 Diffusion Controlled Coarsening. The simplest relationship of particle size and solubility is for spherical particle of radius r, noncoherent with the matrix, where the interfacial energy, σ, is indepednent of orientation. The relationship is often termed the Thomson-Freundlich equation and is written

$$\ln \frac{c_r}{c_\infty} \approx \frac{2\sigma V_m}{rRT} \tag{16}$$

where c_∞ is the solubility of a particle of infinite radius, c_r is the solubility of a particle of radius r, V_m is the molar volume of the particle. Since in practice, $2\sigma V_m \ll rRT$, it is sufficiently accurate to write,

$$c_r - c_\infty = \frac{2\sigma V_m c_\infty}{rRT} \tag{17}$$

for a growing particle, the rate of change of particle volume, $\frac{dV}{dt}$, is equal to the flux per unit area normal to the particle surface area. The rate of change in particle radius will therefore be given by,

$$\frac{dr}{dt} = - DV_m \left(\frac{dc}{dr}\right)_r \tag{18}$$

where D is the diffusion coefficient of the component of the dispersed phase in the matrix, $\left(\frac{dc}{dr}\right)_r$ is the concentration gradient at the surface of the particle. If the volume fraction of the dispersed phase is sufficiently dilute, the

concentration gradient at the particle surface can be approximated by Zener's solution[45] for the stationary diffusion flux to a spherical particle of radius r. Thus from the equation (18)

$$\frac{dr}{dt} = - \frac{DV_m}{r} (c_r - c) \qquad (19)$$

where c is the concentration of the dissolved component in equilibrium with a particle of critical radius, r*, which neither grows nor dissolves. When the particle solubility is small, the total volume of the particles is constant, independent of particle-size distribution. This may be expressed as,

$$4\pi\Sigma r_i^2 \frac{dri}{dt} = 0 \qquad (20)$$

where the summation is taken over all the particles i of the system. Combining equations (19) and (20) with the Thomson-Freundlich equation (17), one can write,

$$\frac{dr}{dt} = \frac{2Dc_\infty \sigma V_m^2}{rRT} \left[\frac{1}{r^*} - \frac{1}{r} \right] \qquad (21)$$

It is apparent from the equation (21) that $\frac{dr}{dt}$ will be positive for particles of radius larger than r* and negative for smaller ones. Particles of radius equal to the mean radius, ($\bar{r}$), are neither growing nor dissolving, and hence, $r^* = \bar{r}$. A particle size distribution function, f(r, t), may be defined such that f(r, t) dr is the number of particles at time t having radii between r and r+dr. The distribution function must obey a continuity equation of the form,

$$\frac{\partial f}{\partial t} = \frac{\partial (\frac{dr}{dt}) f}{\partial r} = 0 \qquad (22)$$

solving the differential equations (21) and (22), it has been shown by Wagner[42] that the average particle size, $\bar{r}$ follows a simple time law,

$$\bar{r}(t)^3 - \bar{r}(o)^3 = \frac{8Dc_\infty \sigma V_m^2}{9RT} t \qquad (23)$$

The distribution function in the normalized variable, $\frac{r}{\bar{r}} = \rho$ takes the form,

$$f(\rho, t) \propto \rho^2 \left(\frac{3}{3+\rho}\right)^{\frac{7}{3}} \left(\frac{\frac{3}{2}}{\frac{3}{2} - \rho}\right)^{\frac{11}{3}} \exp\left(-\frac{\rho}{\frac{3}{2} - \rho}\right),$$

$$\text{when } 0 < \rho < \frac{3}{2}$$

$$f(\rho, t) = 0, \text{ when } \rho > \frac{3}{2} \qquad (24)$$

A plot of the steady-state size distribution is shown in Figure 10(a) and implies a sharp cut-off in the distribution such that no particles exist at long times that have a radius greater than 1.5 times the mean radius of the distribution. It is noteworthy that after prolonged coarsening when the system has attained its steady-state, the size distribution given by equation (24) is independent of initial particle size distribution.

In the foregoing sections the situation where the particles consisted of a pure component was considered. However when the coarsening of compound precipitates is considered, the particles consist of more than one component, and exchange of matter between the particles is subject to a "composition constraint". To maintain the correct chemical composition of the particles, the fluxes of the components must be coupled. This may be done by defining an effective diffusion constant, D_{eff}. For the general case of diffusion controlled coarsening of compound precipitate A_aB_b the fluxes of components A and B will be in the ratio of a:b and an effective diffusion constant may be defined as:[44]

$$D_{eff} = \frac{D_A D_B (C_A C_B)^{\frac{1}{2}}}{C_A D_A b^2 + C_B D_B a^2} \qquad (25)$$

where D_A and D_B are the diffusivities of the components A and B respectively and C_A and C_B are the concentrations of A and B expressed in moles per cm^3.

The theories of coarsening originally were developed for fluid matrices. In a solid matrix, one has the extra condition that space must be made for the growing particles and that no voids should appear at the shrinking particles. In the absence of plastic deformation, a "volume constraint" is

imposed on the coupled diffusive fluxes of the matrix and particle atoms. If V_1 is the volume made available by the transfer of one gm-atom of component 1 from the particle to the matrix and $\bar{V}_2$ is the partial molar volume of component 2 in the matrix then an effective diffusion coefficient for component 1 subject to volume constraint may be defined as:[44]

$$D_{1\ eff} = \frac{C_2 D_1 D_2 \bar{V}_2 (\bar{V}_2 + \frac{C_1}{C_2} V_1)}{C_2 D_2 \bar{V}_2^2 + C_1 D_1 V_1^2} \tag{26}$$

It is not difficult to extend the definition of an effective diffusion constant to the case of both composition and volume constraint and to the case where there is an excess of either component. Hence for the case of diffusion controlled coarsening of compound precipitates in a rigid matrix, an effective diffusion constant should be defined and employed in the expression for the rate constant of coarsening.

2.1.2 Reaction Controlled Coarsening. Wagner[42] in his treatment of reaction controlled coarsening assumed that the rate of transfer of atoms is proportional to the difference between the equilibrium concentration c_r at a particle of radius r (given by the Thomson-Freundlich equation) and the average concentration r* of the solute. Thus for a particle with radius r,

$$\frac{dr}{dt} = - K_I V_m (c_r - c^*) \tag{27}$$

where K_I is the reaction rate constant at the interface. As in the case of diffusion control, using the equations (17), (20) and (27), one can write,

$$\frac{dr}{dt} = \frac{2K_I \sigma V_m^2 C_\infty}{RT} \left[\frac{1}{r^*} - \frac{1}{r}\right] \tag{28}$$

Solving the two differential equations (22) and (28) it may be shown that the critical radius has the time dependence,

$$r^*(t)^2 - r^*(o)^2 = \frac{K_I C_\infty \sigma V_m^2}{RT} t \tag{29}$$

The critical radius r* can be shown[43] to be equal to $\frac{9}{8}\bar{r}$ so that,

$$\bar{r}(t)^2 = \bar{r}(o)^2 = \frac{64\ K_I C_\infty \sigma V_m^2}{81\ RT} \qquad (30)$$

The distribution function takes a simple form when the particle radii are expressed in the reduced quantity $\rho = \frac{r}{\bar{r}}$. It is found that,

$$f(\rho, t) \propto \rho\ \left(\frac{2}{(2-\rho)}\right)^5\ \exp\ \left(\frac{-3\rho}{2-\rho}\right)$$

$$\text{when } 0 < \rho < 2$$

$$f(\rho, t) = 0 \text{ when } \rho < 2 \qquad (31)$$

Again there is a cut-off in the particle size distribution, which now occurs at a particle radius equal to twice that of the particle which is neither grcwing nor dissolving at that instant. A plot of the size distribution is given in Figure 10(b).

2.2 Experimental Studies of Oxide Coarsening in Metals

Seybolt[46] has reviewed the available data on the coarsening of oxide dispersions in a metallic matrix and discussed the factors which influence the coarsening rate. The results of the experimental investigations of particle coarsening in three systems, viz., Ni-Al_2O_3,[47,48] Fe-Al_2O_3,[49] Cu-SiO_2[50] were examined, and comparisons were made between the experimentally observed rates of coarsening and the rate calculated from the Lifshitz-Wagner equation for volume-diffusion controlled coarsening. The agreement was surprisingly good despite some uncertainties in estimating the values of the solubility of the rate-controlling species and the particle-matrix interfacial energy. Seybolt points out that the solubility of the rate-determining species will be determined by the solubility product of the oxide in the metal matrix. It will also be a function of the oxygen activity which is determined by the partial pressure of oxygen in the gas phase at a constant temperature. The possibility of diffusive coupling was considered but it was found that the assumption of rate control by metal (Si or Al) diffusion gave as good a fit to the experimental observa-

tions as the diffusive coupling model. The calculations made assuming oxygen diffusion provided coarsening rates appreciably larger than those observed.

Williams and Smith[51] investigated the coarsening of silica and titania particles in vacuum in internally oxidized Cu-Si and Cu-Ti alloys respectively. While the coarsening behavior of the former was volume-diffusion controlled, the latter did not show any appreciable coarsening initially and significant coarsening was observed only after 200 hours of annealing at 1000°C. If this was taken at time, t=0, reasonable agreement was found with a $t^{1/3}$ law, indicating diffusion controlled coarsening. This tranisition from the stabilization of the oxide particles to sudden coarsening was associated with the loss of coherency at the oxide particle-matrix interface. Since the driving force for coarsening is larger for incoherent than for coherent interfaces, the coarsening rate is greatly increased once coherency is lost. A pre-worked alloy showed particle coarsening at all times approximating a $t^{1/3}$ law and Williams[51] considered that cold working had destroyed the coherency of the interface, thus giving a higher driving force for coarsening at all periods. Later work on this system by Woolhouse and Brown[52] revealed that the titania particles are incoherent right from the beginning. They explained the results of Williams and Smith[51] in terms of impurity effects.

Faulkner[53] investigated the thermal stability of alumina particles in Ni-Al_2O_3 and Ni-Al_2O_3-Mg alloys at 1300°C in a hydrogen atmosphere. A diffusion-controlled coarsening mechanism was found to be rate determining for magnesium-free alloys. However, for the Mg-containing alloys this was not the case. The initial growth rate was found to be much faster than that possible by the diffusion-controlled mechanism. After about 16 hours, however, the coarsening process came to a virtual halt. Since no major changes in the interfacial energy were noted, this type of behavior was attributed to the reduction of the diffusivity of the slowest moving species in the matrix.

Perry and Smallman[54] commented on Faulkner's work and presented some coarsening data for alumina particles in a Ni-Al_2O_3-Mg alloy in vacuum at 1200°C. The addition of Mg was found to increase the coarsening at a continuous rate without any stabilization of the oxide particles. The exponent, n, for the coarsening equation, $\bar{r}^n - r_o^n = Kt$, was not determined conclusively, since the values of n=2, 3 or 4 all gave equally good fit to the data. EMMA investigations were carried out to determine the Mg distribution and indicated the Mg was mainly associated with alumina particles. The possible effects of Mg, upon the parameters in the Lifshitz-Wagner equation, in particular the interfacial energy, the formation of a mixed oxide, and the possible reduction of alumina by Mg were discussed, but no clear model was proposed for the coarsening of alumina particles in Ni-Al_2O_3 alloys.

Fischmeister and Navara[55] have shown that the addition of alloying elements could have a strong influence on the coarsening rate of alumina dispersions in metallic matrices, such as, Ni and Fe. The observed effects were explained by the interaction of alloying elements with the oxide phase. For instance, Mn increases the coarsening rate by forming a spinel phase ($MnAl_2O_4$) of lower structural stability. It is also possible that the interfacial energy is raised by a change of the atomic arrangement at the interface, but this effect was not explored. The authors have further shown that the addition of Cr, Mo and Ti to the Ni-Al_2O_3 alloy decreases the coarsening rate of the oxide particles by lowering the interfacial energy coupled with perhaps a decrease in the concentration of the rate-determining species. The alumina particles extracted from the Ni and the Fe matrices with the addition of Cr, Mo and Ti showed some color changes, x-ray fluorescence and changes in the lattice parameter, indicating that the oxide phase has taken some of the additions into solid solution.

Bhattacharyya and Russell[56] proposed, based on thermodynamic arguments, that the activation energy of coarsening, Q_c, for diffusion-controlled coarsening of compound precipitates cannot in general be identified with the activation energy for diffusion of either component. Instead, Q_c is a very sensitive function of the atmosphere of coarsening and will include terms involving the heat of solution of the compound precipitate in the matrix plus contributions from other processes depending on whether coarsening is conducted in a closed system or in a reactive atmosphere. The same authors[57] extended their theory to study the coarsening kinetics of silica in copper for a range of temperatures and partial pressures of oxygen. Reasonable agreement was found when the coarsening was conducted in an atmosphere wherein the partial pressure of oxygen, controlled by a mixture of copper and cuprous oxide, varied with the temperature of coarsening. In other cases, where the coarsening was conducted in an atmosphere of fixed partial pressure of oxygen, the agreement was poor. The authors attributed this to the fact that the equilibrium between the oxygen dissolved in the coarsening specimens and gaseous oxygen at fixed partial pressure was never attained within the allotted times of coarsening.

The present work is comprised of a careful study of the structure and morphology of TiO_2 precipitates formed in Cu by internal oxidation and the coarsening rates and mechanism of these precipitates as influenced by temperature and oxygen partial pressure.

B. Experimental Procedure

1. Alloy Preparation

The alloy used in this portion of the study was Cu-0.25 wt pct Ti which was prepared and internally oxidized as described in Section I.A.2.

The as-oxidized materials were mechanically polished from one side until the thickness of the strip specimens was about 0.125 mm. This was necessary to eliminate the solute depleted zone from the center of the specimen and also to remove as much as possible any variation in particle sizes produced by

the method of internal oxidation. The specimens were lightly etched in dilute nitric acid to remove the deformed layer from the surface formed during mechanical polishing. The long-term coarsening experiments were carried out at 900°C, 950°C, and 1000°C, using the as-oxidized specimens. One set of samples consisting of three specimens was individually sealed in evacuated Ti-gettered, quartz capsules. In order to ensure a virtually oxygen-free atmosphere inside the capsule, the titanium chips were heated to red heat until virtually all the oxygen was gettered out. The purpose of this was to carry out the coarsening experiment in an atmosphere of low oxygen partial pressure over the alloy. The other set of samples also consisting of three specimens were packed in a powder mixture consisting of equal volumes of cuprous oxide, copper and alumina powders and heated under vacuum in quartz capsules. This fulfilled the condition of performing the coarsening experiment in an atmosphere where a definite oxygen partial pressure could be maintained over the alloy. The partial pressure of oxygen thus established over the alloy would also be the highest permissible without oxidizing the copper matrix.

2. Specimen Preparation for Electron Metallography

For microscopic examination of the oxide-dispersed structures, the carbon extraction replica method was used in conjunction with the thin foil method. The former was used mainly for the identification of the oxide particles and for the measurement of the oxide particle size distribution, whereas the latter was employed to observe the matrix substructure containing the oxide particles, grain boundary precipitates, and various contrast effects arising from the interactions between the particles and the matrix.

3. Quantitative Metallography

3.1 Particle Size Measurement

The extraction replica method was chosen for determining the particle size distribution and for calculating the mean size of the dispersion of oxide particles. Four or five photographs were taken from several replicas prepared

from different regions of the sample. While taking photographs care was taken to avoid areas which were not truly representative of the particle size distribution. These were the areas near the grain boundaries, where precipitate depleted zones may be expected, and also regions where some clustering of particles was observed. At least 200 particles were measured for each sample. The particles were grouped according to their sizes and a histogram of cumulative frequency versus particle size was constructed to plot the particle size distribution and to calculate the mean size of the dispersoid.

3.2 Measurement of Dihedral Angles from Grain Boundary Precipitates

The thin foil method was employed to observe the grain boundary precipitates and for estimation of the Cu/TiO_2 interfacial energy. Those grain boundary precipitates exhibiting faceting were carefully avoided since the presence of facets would indicate that an orientation-independent precipitate-matrix boundary has not been attained. Therefore only lenticular-shaped grain boundary particles were observed. To obtain a reliable estimate of the precipitate-matrix interfacial free energy it is first necessary to measure the true dihedral angles. Therefore, before any photograph was taken the foil was tilted to align the grain boundary plane approximately parallel to the electron beam. The minimization of grain boundary fringe width satisfied this condition. Prints were made and the dihedral angles were measured from the photomicrographs.

C. Results and Discussion

1. Particles in As-Oxidized Alloys

The results of this portion of the project have been reported previously[24,58] and will only be outlined here.

a. The crystal structure of the oxide particles was found to correspond to the rutile modification of TiO_2 for oxidation temperatures above 850°C and to the anatase structure for temperatures below 800°C. The two structures

were found to coexist between 800 and 850°C.

b. Both the rutile and anatase particles exhibited definite orientation relationships with the Cu matrix.

c. The average TiO_2 particle size near the surface of the specimens varied from 76 A° for Cu-0.25 wt pct Ti oxidized at 750°C to 370 A° for 1.0 wt pct Ti oxidized at 1000°C.

d. The particle size was found to increase linearly with depth below the specimen surface.

e. The interfacial free energy for the Cu/TiO_2 interfaces was found to lie in the range 400-700 ergs/cm^2 from dihedral angle measurements for grain boundary precipitates.

2. Coarsening

The coarsening of TiO_2 dispersions in Cu has been studied in two different atmospheres of differing oxygen partial pressures in the temperature range 900 to 1000°C.

One set of experiments was conducted in vacuum, where a low partial pressure of oxygen was maintained over the specimens by gettering the oxygen with titanium chips. In the other the highest possible partial pressure of oxygen which would not oxidize the copper was achieved by packing the specimens in a powdered mixture of Cu and Cu_2O. The coarsening behavior indicated that the inherent thermal stability of the titanium oxide particles is extremely good. The oxide dispersions were very resistant to coarsening during prolonged high temperature annealing. A typical electron micrograph is shown in the Figure 11 where the oxide particles were coarsened in vacuum. The morphology of the oxide particles was found to be roughly spherical throughout the process of coarsening. Electron diffraction studies identified the structure of these particles to be TiO_2 (rutile).

The oxide particle sizes were measured from electron micrographs obtained for each heat treated specimen. The arithmetic mean diameter and the standard deviation for the particle size distribution were calculated

from each set of measurements. The size distributions were constructed by grouping the particle diameters within an interval of 25 A^{o}. The relative frequency of occurrence for each group was estimated and plotted against the particle size. The resultant histogram of particle sizes reveals the variation of the number of particles per unit area with the continuation of the coarsening process. A representative set of histograms is shown in Figure 12, where the coarsening of the oxide particles was conducted in vacuum at a temperature of 954^{o}C. The particle size distribution for the "as-oxidized" material has also been included in this figure to serve as a comparison. The particle size distribution initially seems narrow but gradually broadens as coarsening proceeds. An increasing number of particles with less than the average size of the particle assembly start to dissolve and ultimately disappear. The distribution curves do not follow the steady state particle size distribution predicted by the Lifshitz-Wagner theory of coarsening. Instead all of the size distributions exhibit a long tail towards the large sizes. The particle size distribution is observed to be very similar to the log-normal distribution for the entire range of coarsening times examined at all temperatures. The log-normal distribution may be approximately verified if a symmetrical normal curve yields by plotting of the frequencies against the log of the particle size. However, for a rigorous test of such a distribution, the cumulative frequencies plotted against particle size should lie about a straight line[59] when plotted on log-normal probability paper. This is shown in Figure 13 where the particle size distributions obtained from the histograms in Figure 12 have been replotted on log-normal probability paper. The plots are shown to be straight lines although for long term coarsening experiments (996 hours at T = 954^{o}C in vacuum) there is a slight deviation from linearity at the large particle end of the distribution. Two straight lines of different slopes could be drawn to fit the points on the probability paper. Similar histograms for the particle size distribution for specimens coarsened in Cu/Cu_2O at

T = 951°C are shown in Figure 14 and Figure 15 respectively.

To establish the rate controlling step for the coarsening process, it is customary to plot the experimental results by assuming the existing rate laws of coarsening and subsequently determining where the best fit might be obtained. For example, the difference between the rate equations for interface and for diffusion controlled coarsening rests in the power to which the mean diameter, $\bar{d}$, must be raised to bear a linear relationship with time. In interface control, the rate equation shows a linear dependence between $\bar{d}^2$ and time, whereas the case of diffusion controlled coarsening $\bar{d}^3$ is proportional to time. The departure from linearity in any of the plots indicates that a wrong exponent of the mean diameter has been chosen or that an alternative relationship is required to describe the rate controlling step for the coarsening process. If the initial average size of the oxide dispersion is negligible during the onset of coarsening, it is appropriate to present results as a logarithmic plot of the variation of the mean particle diameter with time and determine the correct exponent of the particle diameter. This is not however the case under the present conditions, since the average diameter of the oxide dispersion before coarsening is of the order of 85 A°.

It is found that a $\bar{d}^3$ versus time plot gives the best fit to most of the experimental data. Figure 16 shows the resulting plots for coarsening in Cu/Cu_2O giving a linear form with correlation of better than 0.99. Figure 17 shows a similar plot for coarsening under vacuum. The latter results show some scatter. It was however found that any other relationship (such as, $\bar{d}^2$ proportional to time, for interface-controlled coarsening) resulted in even poorer fit to the experimental data. It would therefore appear that under these conditions coarsening of the titanium oxide particles in a Cu matrix is volume diffusion controlled. All the linear plots were fitted to the experimental results by employing the method of least-squares, and the best value for the slope of each individual plot was calculated by performing

a regression analysis on a relationship of the type $\bar{d}^{-3}$ proportional to time. The rate constants for coarsening, K_c, corresponding to a relationship $\bar{r}^{-3} - r_o^{-3} = K_c t$, where r is the particle radius, were further determined by multiplying the slope by a factor of 1/8. Activation energies for the coarsening process, Q_c, were estimated from an Arrhenius plot (Figure 18) of the coarsening rate constants. Table 5 summarizes the various coarsening rates obtained as a function of temperature and atmosphere. The activation energies are also indicated for different atmospheres of coarsening; 53 $\frac{\text{Kcal}}{\text{mole}}$ and 89.4 $\frac{\text{Kcal}}{\text{mole}}$ respectively for vacuum and Cu/Cu_2O.

It appears that the coarsening kinetics of titania particles are diffusion-controlled, as outlined by the Lifshitz-Wagner theory of coarsening, since interface control would indicate a linear dependence between $(\bar{d})^2$ and time. Complete verification of the Lifshitz-Wagner theory of diffusion-controlled coarsening would require that the particle size distribution as predicted by the theory should also be obeyed. The size distributions are much wider than the steady-state particle size distribution predicted by the Lifshitz-Wagner theory for diffusion control and in fact appeared to be very close to log-normal. According to the Lifshitz-Wagner theory for diffusion-controlled coarsening, the particles with diameters greater than 1.5 times the average diameter, $\bar{d}$, should never exist, whereas in the present case a small population of much coarser particles has been observed. This is shown by the long tail obtained in the distribution curve toward the larger particle sizes. The broadening of the particle size distributions is not uncommon and has been observed in several systems, e.g., γ' particles in Ni-base alloys,[60] carbides in steel,[60,61] etc. A completely satisfactory explanation has not yet been provided. It is noteworthy that the steady-state particle size distribution predicted by the Lifshitz-Wagner theory approaches a constant function irrespective of the initial size distribution at the onset of coarsening, although the time to reach the steady state may be different for

different systems. According to Lifshitz and Slyozov[41] for volume-diffusion controlled coarsening the characteristic time to reach steady state is approximately of the order of $\frac{\bar{d}_o^3}{K_c}$, where $\bar{d}_o$ is the average particle size at the onset of coarsening and K_c is the rate constant for coarsening. In the Cu-TiO_2 system, where the coarsening rates are extremely slow, the steady-state may never have been reached within the allotted times of coarsening.

The metallographic observation of the microstructure of the coarsened alloy reveals that only a small population of much coarser particles has resulted in a broader distribution of particle sizes than is predicted by the Lifshitz-Wagner theory. The observations suggest that these particles ripened by a mechanism which is different from volume diffusion control. A probable cause is that dislocations are always present in internally oxidized alloys and may influence the kinetics of coarsening. Such dislocations are usually introduced during quenching from a high temperature due to thermal stresses. It is probable that during coarsening at high temperatures, the mobile matrix dislocations would be attracted to some of the oxide particles through intersection of strain fields and these particles would coarsen through dislocation pipe diffusion. Although thin foil micrographs have not clearly revealed the coarser particles to be associated with dislocation lines, it is quite likely that the dislocation images might not have been resolved by the usual two-beam technique of imaging particles and high resolution weak-beam dark field imaging using a matrix reflection is necessary to show the dislocation lines more clearly.

Since it is the purpose of this investigation to assess the theory of particle coarsening in a quantitative manner, the experimental rate constants of coarsening must be compared with the predictions of the Lifshitz-Wagner theory. For Cu/Cu_2O, the coarsening of the titanium oxide particles was observed to be diffusion-controlled. However, to correlate the experimental

coarsening rate of a compound precipitate, such as TiO_2, from the existing physical-chemical parameters the rate controlling species must be identified. The decisive factor is the product of diffusivity and solubility and the component with the minimum value of this product will be rate controlling. The diffusion coefficient of oxygen in copper[63] is about three orders of magnitude faster than that of Ti[64] and for coarsening at the highest possible partial pressure of oxygen, it is very likely that titanium would be rate controlling. The rate constant for coarsening may therefore be written as,

$$K_c = \frac{8}{9RT} (C_{Ti} C_O)^{\frac{1}{2}} (D_{eff}) \sigma (V_{TiO_2})^2 \qquad (32)$$

where C_{Ti} and C_O are concentrations titanium and oxygen expressed in moles/cm^3, σ is the interfacial free energy for the precipitate-matrix interface, V_{TiO_2} is the molar volume of the TiO_2 oxide and D_{eff} is the effective diffusivity for the case of mass transport through the matrix under compositional constraint[44] and is given by,

$$D_{eff} = \frac{D_{Ti}^{Cu} D_O^{Cu} (C_{Ti} C_O)^{\frac{1}{2}}}{4 C_{Ti} D_{Ti}^{Cu} + C_O D_O^{Cu}} \qquad (33)$$

For the case of titanium oxide dispersed in a Cu matrix, where the diffusivity of oxygen, D_O^{Cu}, is generally very much greater than that of the titanium, D_{Ti}^{Cu}, this reduces to

$$D_{eff} \simeq \frac{D_{Ti}^{Cu} (C_{Ti} C_O)^{\frac{1}{2}}}{C_O}, \quad D_O^{Cu} >> D_{Ti}^{Cu} \qquad (34)$$

Therefore, substituting the above in equation (32), gives

$$K_c = \frac{8}{9RT} D_{Ti}^{Cu} C_{Ti} \sigma V_{TiO_2}^2 \qquad (35)$$

The diffusivity of Ti in Cu has been reported in the literature[64] but the solubility of titanium in a system such as, Cu-TiO_2, is not available and cannot be calculated, since the solubility product of TiO_2 in Cu is unknown. Therefore an attempt was made to calculate the solubility term from elementary thermodynamic principles and is shown in Appendix C. The interfacial energy term was calculated from the measurement of the dihedral angles formed with grain boundaries in the Cu matrix by lenticular-shaped TiO_2 oxide particles

and was found to lie between 400 to 700 ergs/cm^2. [24] The molar volume of the TiO_2 oxide was calculated from the specific gravity[65] and molecular weight of TiO_2 (rutile) as 18.84 cm^3/mole.

At three different temperatures of 900°C, 951°C and 1000°C, the calculated rates of coarsening in Cu/Cu_2O are $0.026 \times 10^4 \frac{A^{o3}}{sec}$, $0.095 \times 10^5 \frac{A^{o3}}{sec}$ and $0.247 \times 10^6 \frac{A^{o3}}{sec}$ respectively. If these are compared with the experimental rates given in Table 5B, the estimated rates appear to be 4 to 6 orders of magnitude higher than the experimental values. The sources of error in estimating the various physiocochemical factors are probably the greatest in the determination of the solubility-product data in Cu. The solubility of titanium in contact with the TiO_2 oxide particles dispersed in the Cu matrix has been calculated by assuming regular behavior of the ternary Cu-Ti-O solution and by neglecting the mutual interaction effects of titanium and oxygen on their activities in copper. The calculated value of the solubility of Ti could very well be affected by the above assumptions and a more precise value cannot be obtained unless independent experiments are performed to determine the solubility product and heat of solution of the oxide precipitate in the Cu matrix.

Seybolt[46] determined the solubility product of silica in Cu by equilibrating "six nine" purity Cu in a quartz tube in a 10^{-6}mm vacuum at 1000°C for 94 hours. The determination of the solubility product was possible by the subsequent chemical analysis for oxygen and silicon content dissolved in Cu. The estimated value of the solubility product was thus equal to 7.2×10^{-17} at 1000°C. The solubility product, K_s, is related to the heat of solution of the precipitate in the matrix by a relation of the type $K_s = (\text{Const}) \exp\left(-\frac{\Delta Hs}{RT}\right)$, where ΔHs is the heat of solution and the constant is related to the corresponding change in entropy when a mole of pure, compound precipitate dissolves and dissociates. If the entropy change is assumed to be negligible, the heat of solution of 1

mole of SiO_2 in Cu can be estimated to be equal to 95 $\frac{Kcal}{mole}$. In the absence of any oxide solubility-product data for the Cu-TiO_2 system, this value of 95 $\frac{Kcal}{mole}$ may be taken as the enthalpy of solution of TiO_2 in Cu. This is not unreasonable considering the fact that the solubility product is a strong function of the free energy of formation of the compound, and both the oxides of Si and Ti possess standard free energies of formation, ΔG^o, that are not too different from one another. Thus the number of moles/cm^3 of titanium in solution in copper, C_{Ti}, can be calculated from the solubility product and from the moles/cm^3 of oxygen dissolved in copper.[63] The coarsening rate constant as given by the equation (35) may be estimated for different temperatures. The calculated rates now become 0.688 $\frac{A^{o3}}{sec}$, 6.4 $\frac{A^{o3}}{sec}$, 48.04 $\frac{A^{o3}}{sec}$ at the temperatures of 900°C, 951°C and 1000°C respectively. Comparing these with the experimentally determined values given in Table 5B reveals that the estimated values are a factor of 24 to 84 higher than the experimentally determined values. Thus the agreement is reasonably good with the Lifshitz-Wagner theory of diffusion-controlled coarsening despite the uncertainties involved inthe calculation of the solubility term.

In order to estimate the activation energy for the coarsening process, Q_c, the rate constant may be expressed as a preexponential term and an activation energy. Thus from equation (35), K_c, the rate constant for Ti-diffusion controlled coarsening can be written as,

$$K_c = \frac{8}{9RT} D_{Ti}^{Cu} C_{Ti} \sigma V_{TiO_2}^2 = K_o \exp\left(-\frac{Q_c}{RT}\right) \qquad (36)$$

From the equality given in the middle the only temperature dependent terms in equation (36) are the diffusivity and the solubility including the temperature factor in the denominator. Taking 'ln' of both sides and differentiating with respect to $\frac{1}{T}$, the expression for the activation energy of coarsening, Q_c,

is obtained as follows,

$$Q_c = Q_C^{Ti} - R \frac{d\ln C_{Ti}}{d(\frac{1}{T})} - RT \qquad (37)$$

where Q_C^{Ti} is the activation energy of diffusion of Ti in Cu. The evaluation of $\frac{d\ln C_{Ti}}{d(1/T)}$ will depend on the environment[56] in which the coarsening is carried out. For infinitely dilute solutions of Ti and O in Cu, Henry's law may be valid, and the solubility of Ti in equilibrium with TiO_2 in Cu is related by the well known equation,

$$(C_{Ti})(C_O)^2 = K_s^{TiO_2} = (\text{Const}) \exp\left(-\frac{\Delta Hs}{RT}\right) \qquad (38)$$

where $K_s^{TiO_2}$ is the solubility product of TiO_2 in Cu and ΔHs is the heat of solution of 1 gm mole of TiO_2 dissociating into 1 mole of Ti and 2 moles of O in solution in Cu.

Since coarsening is conducted in the presence of Cu and Cu_2O, enclosed in the same capsule, the partial pressure of oxygen would vary with the temperature of coarsening. Equilibrium will be established between the gaseous oxygen evolved from the dissociation of Cu_2O and atomic oxygen dissolved in Cu containing the dispersed phase of TiO_2 oxide particles. The corresponding chemical reaction is represented by the following:

$$Cu_2O_{(s)} \leftrightarrow 2Cu_{(s)} + \underline{O} \text{ (in Cu)} \qquad (39)$$

The concentration of O in solution may be expressed as,

$$C_O = (\text{Constant}) \exp \frac{-(\Delta\bar{H}_O - \Delta H^o_{Cu_2O})}{RT} \qquad (40)$$

where $2\Delta\bar{H}_O$ is the heat of solution of one gm mole of gaseous oxygen in Cu and $\Delta H^o_{Cu_2O}$ is the standard heat of formation of Cu_2O from its elements. Substituting C_O from equation (40) into equation (38), one obtains for the concentration of Ti dissolved in Cu as,

$$C_{Ti} = (\text{Constant}) \exp \frac{(-\Delta H_s + 2\Delta\bar{H}_O - 2\Delta H^o_{Cu_2O})}{RT} \qquad (41)$$

$$\text{or, } \frac{d\ln C_{Ti}}{d(\frac{1}{T})} = \frac{-\Delta H_s + 2\Delta\bar{H}_O - 2\Delta H^o_{Cu_2O}}{R} \qquad (42)$$

Substitution of equation (42) into equation (37) (and neglecting the insignificant 'RT' term in equation (37)) yields the activation energy of coarsening as follows:

$$Q_c = Q_D^{Ti} + \Delta H_s - 2\Delta\bar{H}_O + 2\Delta H^o_{Cu_2O} \qquad (43)$$

In order to estimate Q_c, Q_D^{Ti} is known[66] and is equal to 63 Kcal/mole and as mentioned previously ΔH_s can be approximated to be equal to 95 $\frac{\text{Kcal}}{\text{mole}}$. The enthalpy of solution of oxygen in solid Cu, $\Delta\bar{H}_O$, has been evaluated by Pastorek and Rapp[63] and is equal to -10 $\frac{\text{Kcal}}{\text{mole}}$. $\Delta H^o_{Cu_2O}$ is also tabulated in the literature[67] and is equal to -40.2 $\frac{\text{Kcal}}{\text{mole}}$. The calculated value of Q_c from equation (43) is thus equal to 97.6 $\frac{\text{Kcal}}{\text{mole}}$, whereas the experimentally determined activation energy is 89.4 $\frac{\text{Kcal}}{\text{mole}}$. Thus the agreement is fairly reasonable considering the uncertainty involved in the estimation of the heat of solution, ΔH_s, and other calculated energy terms.

Analysis of the coarsening data in the vacuum case reveals that the coarsening rate is higher than the Cu/Cu_2O atmosphere at least for the lower temperatures of coarsening, i.e., at T = 900°C, but this no longer remains true at higher temperatures. At first this seems surprising, since through the requirement of fixed solubility product of the oxide in the metallic matrix, coarsening at a lower partial pressure of oxygen would ensure a relatively greater amount of titanium dissolved in the copper matrix. If the coarsening is indeed Ti-diffusion controlled, the oxide particles will be ripening at a much faster rate in vacuum where the oxygen activity in the surrounding atmosphere has been maintained at a low level by using the Ti-chips as the oxygen getter. On the other hand keeping the oxygen activity very low may lead to a switch from titanium to oxygen as the rate controlling species for the diffusion-controlled coarsening. The decisive term as to which is

rate controlling in the vacuum case is of course the diffusivity-solubility product. In the absence of the solubility-product data and the lack of knowledge of the exact oxygen activity in the gas phase for the vacuum case, the determination of dissolved oxygen in Cu is not possible. However in the presence of a strong oxygen getter such as Ti, and assuming the permeation of oxygen through the evacuated quartz capsule to be negligible, the partial pressure of oxygen in the gas phase could be taken as near zero. Exactly by what proportion the partial pressure of oxygen will be reduced, is to be determined from the equilibrium between the dissolved oxygen in the Cu matrix and the gas phase. To get an approximate idea of the partial pressure, the thermochemical behavior of the Ti-O system is considered. Oxygen has a significant solubility in Ti, and Ti forms a series of condensed oxide phases among which the losest oxide is TiO and the highest TiO_2. At a temperature of T = 1300°K, the corresponding partial pressures of oxygen at which these oxide species first begin to form range from 10^{-33}atm to 10^{-19}atm respectively.[68] Assuming Sieverts law to be valid, the average atom fraction of oxygen dissolved in Cu at T = 1300°K would be on the order of 10^{-13}. Therefore, at such low concentration of dissolved oxygen in the matrix, the diffusivity-solubility product for oxygen will be several orders of magnitude lower than for Ti, although the atomic mobility of oxygen is about three times greater than that of Ti in Cu. Thus under these circumstances oxygen will be the rate controlling species for coarsening. For the case of oxygen-diffusion controlled coarsening, the rate constant can be derived from equation (33) and may be written as,

$$K_c = \frac{2D_O^{Cu} C_O \sigma V_{TiO_2}^2}{9RT} \qquad (44)$$

The diffusivity of oxygen in Cu, D_O^{Cu}, is well known,[63] σ and V_{TiO_2} are as before. Using equation (44) and from the experimental values of coarsening rate constants in vacuum as given in Table 5A, one may estimate the concentration of dissolved oxygen in Cu. In this way, the concentration of dissolved oxygen in Cu is on the order of 10^{-14}, in fair agreement with the proposed theory of oxygen-diffusion controlled coarsening.

To calculate the activation energy of coarsening, equation (37) may be utilized with the exception that oxygen is the rate controlling species. Therefore, neglecting the 'RT' term,

$$Q_c = Q_D^O - R \frac{d\ln C_O}{d(\frac{1}{T})} \tag{45}$$

where Q_D^O is the activation energy for the diffusion of oxygen in Cu. The evaluation of $\frac{d\ln C_O}{d(1/T)}$ can be accomplished by considering that gaseous oxygen in the surrounding atmosphere is equilibrated with the atoms of oxygen dissolved in the Cu matrix, through the following reaction:

$$\tfrac{1}{2}O_{2(2)} = \underline{O} \text{ (in Cu)} \tag{46}$$

The concentration of dissolved oxygen is related to the partial pressure as,

$$C_O = \text{Const } p_{O_2}^{\frac{1}{2}} \exp\left(-\frac{\Delta\bar{H}_O}{RT}\right) \tag{47}$$

where $2\Delta\bar{H}_O$ is the heat of solution per gm mole of gaseous oxygen in Cu. If the partial pressure of oxygen is assumed to be constant during the coarsening process,

$$\frac{d\ln C_O}{d(\frac{1}{T})} = -\frac{\Delta\bar{H}_O}{R} \tag{48}$$

Thus from equation (45), the activation energy of coarsening under these conditions is given by,

$$Q_c = Q_D^O + \Delta\bar{H}_O \tag{49}$$

Q_D^O, the activation energy of diffusion of oxygen in Cu is 16 $\frac{Kcal}{mole}$ [63] and $\Delta\bar{H}_O$, the heat of solution of oxygen in solid Cu is given by -10 $\frac{Kcal}{mole}$. The activation energy of coarsening from equation (49) is thus estimated as 6 $\frac{Kcal}{mole}$ compared to the experimentally determined value of 53 $\frac{Kcal}{mole}$.

The discrepancy in the activation energy of coarsening cannot be easily explained since one is unsure of whether or not a constant oxygen activity is closely maintained throughout the coarsening process.

There is comparatively little experimental data available on the quantitative aspects of particle coarsening in oxide-dispersed copper-base systems. The results of the present investigation may be compared with the work of Bhattacharyya and Russell[57] who performed coarsening experiments as a function of oxygen partial pressure for the Cu-SiO_2 system. Analogous to the present investigation, these authors carried out coarsening at different temperatures in an atmosphere of variable oxygen pressure, wherein the internally oxidized specimen was in intimate contact with the Cu-Cu_2O mixture. The results showed that the agreement between the experimental activation energy of coarsening with the proposed theory was fair. Comparing the coarsening rates of the two oxide-dispersed copper alloys carried out virtually under identical experimental conditions it is observed that the rates differ by about three orders of magnitude with the TiO_2 dispersions being more stable. The reasons for the resistance of the TiO_2 particles to elevated temperature coarsening may be attributed partly to the interfacial energy term and to the solubility term appearing in the expression for the rate constant of coarsening. While the degree of coherency of TiO_2 particles in the Cu matrix is not clear at this juncture, the interfacial energy of these oxide particles is definitely much lower than the amorphous, disordered silica particles in the Cu matrix. The solubility of the rate controlling species (Ti or Si) in equilibrium with the oxide particles in the Cu matrix is also expected to be lower for Ti than Si, probably via a more negative enthalpy of solution of Ti in the Cu matrix.

In an attempt to coarsen silica particles at different temperatures but at a fixed oxygen pressure, the same authors[57] adopted the 'two furnace method', wherein the specimen and the $Cu-Cu_2O$ powder mixture were physically separated, with the latter maintained at a constant temperature. The agreement between the experimental activation energy of coarsening with the theory was considerably poorer under the circumstances and was attributed to the fact that the oxygen in the gaseous phase never equilibrated with the dissolved oxygen in copper. Furthermore, the observed coarsening behavior for the variable and constant oxygen pressure were nearly identical. This points towards the fact that the oxygen dissolved in the copper matrix must have been the same in those two cases and the 'two furnace method' was not suitable for controlling the oxygen partial pressure at a constant level.

III. Mechanical Properties of Internally Oxidized Cu-Ti Alloys

A. Binary Cu-Ti Alloys

The mechanical properties of internally oxidized Cu-Ti alloys have been described in a previous report[58] and will be briefly reviewed here. The tensile data are summarized in Table 6 for four temperatures of internal oxidation. It is found that the TiO_2 dispersion effectively increases the yield strength of Cu-titania alloys by a factor of five to ten over that for pure Cu. Good correlation can be made between the yield strengths and the Orowan mechanism of hardening. Alloys with Ti concentrations of 1 wt pct or less are ductile (15-30 pct elongation). The combined mechanical properties (yield strength and ductility) of polycrystalline Cu-TiO_2 alloys are comparable to the best values yet reported for dispersion strengthened copper.

Fracture of the alloys occurs intergranularly on a plane roughly perpendicular to the tensile axis. Voids are found associated with grain boundary particles at the fracture surface and final fracture occurs by ductile tearing in regions between the voids. The rather low UTS values for the alloys are believed due to this cavitation at grain boundary particles and to dynamic recovery effects.

B. Precipitation and Dispersion Strengthening in Cu-Cr-TiO_2 Alloys

1. Background

The good combination of mechanical properties obtained in internally oxidized Cu-Ti alloys suggested the possibility of combining dispersion strengthening with some other mode of hardening. Such a combination has been studied by Ebeling and Ashby[69] for Cu-Au-SiO_2 and Cu-SiO_2 alloys obtained by internal oxidation in the temperature range 750-1050°C. It was found that the increment in yield strength due to solid solution by the Au was additive to that due to the silica dispersion. Similarly Hirsch and Humphreys[70] found that solid solution and dispersion hardening produced additive effects in Cu-Zn-Al_2O_3 alloys. In the present investigation the combined effects of dispersion

hardening of Cu by a TiO_2 dispersion and precipitation hardening by precipitates of essentially pure Cr were investigated.

2. Experimental Procedure

Binary Cu-0.25 wt pct Ti alloys were internally oxidized at 900°C by the procedure described in section I.A.2. Internally oxidized specimens 0.5 mm thick were chromized by packing in a powder mixture of 80 wt pct Cr and 20 wt pct Al_2O_3, sealing them in quartz tubes under a reduced pressure of argon, and heating for 40 hours at 1000°C. The chromizing treatment introduced 0.21 wt pct Cr into the alloys. The resultant Cu-Cr-TiO_2 alloys were solution annealed under argon in quartz capsules for 3 hours at 995°C and water quenched. Groups of specimens were then aged for various times at 600 and 700°C.

3. Results and Discussion

The 700°C aging curves for a binary Cu-0.20 wt pct Cr and a Cu-0.21 wt pct Cr-TiO_2 alloys are presented in Figure 19. The greater hardness of the TiO_2 dispersed alloy for all aging times is apparent. Transmission electron microscopy has shown that the oxide dispersion has two effects on the precipitation of the Cr-rich phase: a relatively small effect in providing sites for heterogeneous nucleation and a major one in delaying the coherency loss of the Cr precipitates apparently by impeding the motion of matrix dislocations.

The aging temperature of 700°C is rather high for Cu-Cr alloys, however, the effects of the oxide dispersion suggest that further work at lower aging temperatures should be undertaken to optimize the mechanical properties of the alloys.

Conclusions

The results presented in this report allow the following conclusions to be drawn.

1) The kinetics of internal oxidation of Cu-Ti cylinders and spheres may be adequately described using the quasi-steady state approximation even for penetrations which are an appreciable fraction of the specimen radius.

2) The analysis described in Appendix B which includes counterdiffusion of solute gives an accurate description of the kinetics of internal oxidation when more than one oxide forms.

3) Above 850°C the internal oxides formed in Cu-Ti alloys are TiO_2 (rutile) while below 800°C the oxides are TiO_2 (anatase) and between 800 and 850°C the two oxides coexist.

4) The coarsening kinetics of the TiO_2 particles in Cu follow the $\bar{d}^3 \alpha$ time law, characteristic of the *Lifshitz-Wagner theory of* volume diffusion-controlled coarsening.

5) The coarsening rate is significantly slower than that reported for SiO_2 dispersions in Cu.

6) The TiO_2 dispersion effectively increases the yield strength of Cu-titania alloys by a factor of five to ten over that of pure copper. Good correlation can be made between the yield strengths and the Orowan mechanism for dispersion strengthening.

7) Alloys with Ti concentrations of 1 wt pct or less are ductile (15-30% elongation). The combined mechanical properties (strengths and ductilities) of polycrystalline Cu-TiO_2 alloys are comparable to the best values yet reported for dispersion strengthened copper.

8) The combined effects of a TiO_2 dispersion and Cr precipitates on the mechanical properties of Cu indicate a method for obtaining outstanding mechanical properties in Cu alloy systems.

APPENDIX A

Review of Meijering's Analysis of the Kinetics of Internal Oxidation When Two Oxides Form[31]

The internal oxidation of a solute B in a matrix metal A is envisioned to occur in the manner shown in Figure 20. A lower oxide BO_{n_1} forms at the internal oxidation front $x = \xi$. This oxide is then further oxidized, instantaneously, to a higher oxide BO_{n_2} as a second front $x = \eta$ moves through the alloy. The differential equations describing the motion of the two fronts are

$$\frac{D_O N_i}{(\xi - \eta)} = n_1 N_B^{(o)} \frac{d\xi}{dt} \qquad \eta \leq x \leq \xi \tag{A1}$$

$$\frac{D_O (N_O^{(s)} - N_i)}{\eta} = n_1 N_B^{(o)} \frac{d\xi}{dt} + (n_2 - n_1) N_B^{(o)} \frac{d\eta}{dt}$$

$$0 \leq x \leq \eta \tag{A2}$$

where $N_B^{(o)}$ = the atom fraction of solute in the alloy

D_O = the diffusivity of oxygen in the matrix A

t = the oxidation time

$N_O^{(s)}$ = the solubility of oxygen in A

N_i = the oxygen concentration of $x = \eta$

The counterdiffusion of solute is neglected in Eqns. (A1) and (A2).

Division of (A2) by (A1) yields

$$\left(\frac{N_O^{(s)} - N_i}{N_i}\right) \frac{\xi - \eta}{\eta} = 1 + \frac{n_2 - n_1}{n_1} \frac{d\eta}{d\xi} \tag{A3}$$

Since at $t = 0$, $\xi = \eta = 0$ and both ξ and η are proportional to $t^{\frac{1}{2}}$ we have

$$f = \eta/\xi = \frac{d\eta}{d\xi} \tag{A4}$$

in which case Eqn. (A3) may be written as a quadratic

$$\left(\frac{n_2}{n_1} - 1\right) f^2 + \left(\frac{1}{m}\right) f - \left(\frac{1}{m} - 1\right) = 0 \qquad \text{(A5)}$$

where $m = \dfrac{Ni}{N_O^{(s)}} = \sqrt{\dfrac{p_{O_2}^{(n)}}{p_{O_2}^{(o)}}}$

The solution to Eqn. (A5) yields

$$f = \frac{\left[1 + 4m(1-m)\left(\frac{n_2 - n_1}{n_1}\right)\right]^{\frac{1}{2}}}{2m\left(\frac{n_2 - n_1}{n_1}\right)} - 1 \qquad \text{(A6)}$$

Since both η and ξ are proportional to $t^{\frac{1}{2}}$ we may now write

$$\xi^2 = \left(\frac{2N_O^{(s)} D_O}{n_{eff} N_B^O}\right) t \qquad \text{(A7)}$$

where n_{eff}, an effective stoichiometric coefficient, is given

$$n_{eff} = \frac{n_1 (1 - f)}{m} \qquad \text{(A8)}$$

Eqn. (A7) describes the kinetics of internal oxidation of an alloy in which two oxides are formed and allows the calculation of the oxygen permeability in the matrix, $N_O^{(s)} D_O$, from measurements of ξ as a function of t.

APPENDIX B

Determination of $N_O^{(s)} D_O$ from Internal Oxidation Measurements When Two Oxides are Formed and Counterdiffusion of Solute is Important

The analysis to be used is similar to that used by Maak for the case of simultaneous internal oxidation of a solute and external oxidation of the matrix.[39] The concentration profiles of oxygen and solute are shown schematically in Figure 21. It is assumed that

$$\eta = 2 \gamma_2 (D_O t)^{\frac{1}{2}} \tag{B1}$$

and

$$\xi = 2 \gamma_1 (D_O t)^{\frac{1}{2}} \tag{B2}$$

where γ_1 and γ_2 are undetermined constants. The diffusion equation

$$\frac{\partial N_O}{\partial t} = D_O \frac{\partial^2 N_O}{\partial -x^2} \tag{B3}$$

is subject to the boundary conditions

$$N_O = N_O^{(s)}, \; x = 0, \; t \tag{B4}$$

$$N_O = 0, \; x = \xi, \; t \tag{B5}$$

$$N_O = N_i, \; x = \eta, \; t \tag{B6}$$

The solution to (B3) for $\eta \leq x \leq \xi$ is

$$N_O (x,t) = N_i \frac{\text{erf } \gamma_1 - \text{erf} \left[\frac{x}{2 (D_O t)^{\frac{1}{2}}} \right]}{\text{erf } \gamma_1 - \text{erf } \gamma_2} \tag{B7}$$

Similarly the diffusion equation for the solute

$$\frac{\partial N_B}{\partial t} = D_B \frac{\partial^2 N_B}{\partial x^2} \tag{B8}$$

is subject to the initial and boundary conditions

$$N_B = 0, \; x \leq \xi \; , \; t \tag{B9}$$

$$N_B = N_B^{(o)}, \; x \geq 0, \; t = 0 \tag{B10}$$

The solution to (B8) for $x \geq \xi$ is

$$N_B(x,t) = N_B^{(o)} \left[1 - \frac{\operatorname{erfc} \left[\frac{x}{2(D_B t)^{\frac{1}{2}}} \right]}{\operatorname{erfc} \gamma_1 \Theta^{\frac{1}{2}}} \right] \tag{B11}$$

where $\Theta = \frac{D_O}{D_B}$

Substitution of $N_O(x,t)$ and $N_B(x,t)$ into a molar flux balance at $x = \xi$

$$-D_O \left(\frac{\partial N_O}{\partial x}\right)_\xi = n_1 D_B \left(\frac{\partial N_B}{\partial x}\right)_\xi \tag{B12}$$

yields, after rearrangement,

$$N_i D_O = n_1 N_B^{(o)} \frac{\xi (\xi - \eta)}{2t} \frac{1}{F\left[\frac{\xi}{2(D_B t)^{\frac{1}{2}}}\right]} \tag{B13}$$

where the function F is defined by

$$F(\mu) = \pi^{\frac{1}{2}} \mu e^{\mu^2} \operatorname{erfc} \mu$$

$$= 1 - \frac{1}{2\mu^2} + \frac{3}{4\mu^4} \cdots \tag{B14}$$

Eqn. (B13) may be modified to allow calculation of $N_O^{(s)} D_O$ simply by dividing by $m = \frac{Ni}{N_O^{(s)}}$

$$N_O^{(s)} D_O = \frac{n_1 N_B^o}{m} \frac{\xi (\xi - \eta)}{2t} \frac{1}{F\left[\frac{\xi}{2(D_B t)^{\frac{1}{2}}}\right]} \tag{B15}$$

APPENDIX C

Estimation of the Solubility Product of TiO_2 in Cu

The dissolution of titanium oxide particles in a Cu matrix can be represented by the reaction:

$$TiO_{2(Cu)} \rightarrow \underline{Ti}_{(Cu)} + 2\underline{O}_{(Cu)}, \quad \Delta G_s \tag{C1}$$

The knowledge of the free energy change accompanying this reaction as a function of temperature is important for two reasons. First of all, the enthalpy of solution of the titanium oxide in Cu can be evaluated and secondly the solubility product of the compound precipitate can be estimated.

The thermodynamic properties for the ternary Cu-Ti-O solution are limited in the literature. To evaluate the free energy change for the dissolution of titania in Cu from the available thermodynamic data, it is therefore necessary to make certain simplifiying assumptions. One is that the Cu-Ti-O system behaves as a regular solution and the other that the mutual interactions between the atoms of oxygen and titanium dissolved in Cu are to be neglected. The free energy change for the reaction represented by equation (C1) can then be estimated from Hess' law of summation of the following individual reactions:

1. The dissociation reaction of $TiO_{2(s)}$ into its components which are in its pure standard state

$$TiO_{2(s)} = Ti_{(s)} + O_{2(g)}, \quad \Delta G_1^o \tag{C2}$$

2. The dissolution of pure titanium in Cu.

$$Ti_{(s)} = \underline{Ti}_{(Cu)}, \quad \Delta\bar{G}_{\underline{Ti}} \tag{C3}$$

3. The dissolution of gaseous oxygen in Cu.

$$O_{2(g)} = 2\underline{O}_{(Cu)}, \quad 2\Delta\bar{G}_{\underline{O}} \tag{C4}$$

The free energy change for the reaction of interest, represented by the equation (C1) is obtained by the summation as follows:

$$\Delta G_s = \Delta G_1^o + \Delta \bar{G}_{\underline{Ti}} + 2\Delta \bar{G}_{\underline{O}} \qquad (C5)$$

ΔG_1^o, the standard free energy of dissociation of TiO_2 at some absolute temperature, T, is known[68] and can be represented as,

$$\Delta G_1^o = 218458 - 41.72T \qquad (C6)$$

For the evaluation of the free energy chance, $\Delta \bar{G}_{Ti}$, the relative partial molal enthalpy of $Ti_{(s)}$ in solid copper, $\Delta \bar{H}_{Ti}$, is required. Since the activity data in binary Cu-Ti solid alloys are not available, $\Delta \bar{H}_{Ti}$ cannot be readily evaluated. The estimation of the same quantity from the solvus lines of the Cu-rich and the α-Ti solid solutions is possible for the dilute solution case if one neglects the formation of any intermediate phases between the two terminal solid solutions. Using this approximation and considering the equilibrium between the two solid solutions, the ratio of the molefraction of Ti dissolved in Cu, $X_{Ti(sat)}^{(Cu)}$ to the molefraction of Ti in α-Ti, $X_{Ti(sat)}^{(\alpha\text{-}Ti)}$ is plotted as a function of the temperature and is found to be linear. $\Delta \bar{H}_{Ti}$ can thus be estimated from the slope of the curve to be equal to -26090 $\frac{Cal}{mole}$. The entropy of solution of $Ti_{(s)}$ in copper is represented by, $\Delta \bar{S}_{Ti} = -R \ln N_{Ti}$, where N_{Ti} is the atom fraction of Ti. Thus the free energy change for the reaction represented by equation (C3) is

$$\Delta \bar{G}_{Ti} = -26090 + 4.575\ T \log N_{Ti} \qquad (C7)$$

The solubility of gaseous oxygen in solid copper has been treated in some detail by Pastorek and Rapp.[63] These authors determined from electrochemical measurements the solution enthalpy for oxygen in solid copper to be equal to -10,000 Cal/mole. The excess entropy of solution of oxygen was given

as equal to 9.1 k/atom (k = Boltzmann Constant) or 18 Cal/deg mole. The solubility of oxygen in solid Cu was found to follow Sieverts law (solubility proportional to the square-root of the partial pressure of oxygen gas) and at Cu/Cu_2O existence, the solubility was described by the following equation,

$$N_O^{(s)} = 26 \exp\left(-\frac{30200}{RT}\right) \qquad (C8)$$

From equation (C8), the Sieverts law constant may be extracted knowing that the partial pressure of oxygen, as a function of the temperature, at Cu/Cu_2O existence is given by,[68] $p_{O_{2(g)}}^{\frac{1}{2}} = 2.806 \times 10^6 \exp\left(-\frac{30200}{RT}\right)$. Thus the value of this constant is equal to $9.265 \times 10^{-6} \exp\left(\frac{10000}{RT}\right)$. Hence for dilute solutions of oxygen gas in Cu, as long as Henry's law is obeyed, the atom fraction of oxygen in solution with Cu may be expressed as,

$$N_O = 9.265 \times 10^{-6} \exp\left(\frac{10000}{RT}\right) p_{O_{2(g)}}^{\frac{1}{2}} \qquad (C9)$$

The free energy change for the reaction represented by equation (C4) can be evaluated as,

$$2\Delta\bar{G}_O = 2(-10{,}000 + 4.575\ T\log N_O - 18T) \qquad (C10)$$

The free energy change for the reaction represented by equation (C1), ΔG_s, can now be evaluated by substituting the equations (C6), (C7), (C10) into the equation (C5), i.e.,

$$\Delta G_s = 172{,}368 - 77.72\ T + 4.575\ T\ (\log N_{Ti} + 2\log N_O) \qquad (C11)$$

If the matrix is saturated with titanium oxide, the reaction represented by equation (C1) is in equilibrium and the free energy change ΔG_s given by equation (C11) can therefore be set to zero.

$$\text{i.e., } \Delta G_s = 0$$

$$\text{Simplifying, } (N_{Ti})(N_O)^2 = 9.502 \times 10^{16} \exp\left(-\frac{172{,}368}{RT}\right) \qquad (C12)$$

It is now possible to calculate the atom fraction of Ti in solution with the copper matrix containing TiO_2 oxide particles as a function of the temperature and partial pressure of oxygen, by substituting the expression for N_O from equation (C9) in equation (C12). Thus,

$$N_{Ti} = 1.107 \times 10^{27} \exp\left(-\frac{192368}{RT}\right) \frac{1}{p_{O_{2(g)}}} \qquad (C13)$$

The effect of partial pressure of oxygen on the solubility of Ti in equilibrium with the TiO_2-saturated Cu matrix is such that as $p_{O_{2(g)}}$ goes up, the solubility of Ti goes down proportionately.

References

1. R. A. Rapp: Corrosion, 1965, vol. 21, pp. 382-401.

2. J. L. Meijering: Advances in Materials Research, H. Herman, ed., vol. 5, no. 1, pp. 1-81, John Wiley and Sons, Inc., New York, 1971.

3. J. H. Swisher: Oxidation of Metals and Alloys, pp. 235-67, ASM, 1971.

4. G. C. Wood: Oxidation of Metals and Alloys, pp. 201-34, ASM, 1971.

5. J. K. Tien and F. S. Pettit: Met. Trans., 1972, vol. 3, pp. 1587-99.

6. G. S. Ansell: Oxide Dispersion Strengthening, pp. 61-141, Gordon and Breach, New York, 1968.

7. P. B. Hirsch and F. J. Humphreys: Physics of Strength and Plasticity, pp. 189-216, the M.I.T. Press, Cambridge, Mass., 1969.

8. R. Barlow, P. J. Grundy, and B. Johnson: J. Mater. Sci., 1969, vol. 4, pp. 359-69.

9. R. Barlow and P. J. Grundy: J. Mater. Sci., 1970, vol. 5, pp. 1005-10.

10. C. S. Smith: Mining Met., 1932, vol. 13, pp. 481-83.

11. F. N. Rhines, W. A. Johnson, and W. A. Anderson: Trans. AIME, 1942, vol. 147, pp. 205-21.

12. J. L. Meijering and M. J. Dryuvesteyn: Philips Res. Rep., 1947, vol. 2, pp. 81-102,260-80.

13. J. E. Verfurth and R. A. Rapp: Trans. TMS-AIME, 1964, vol. 230, pp. 1310-13.

14. J. Potschke, P. M. Mathew and M. G. Frohberg: Z. Metallk., 1970, vol. 61, pp. 152-55.

15. P. M. Mathew and J. Potschke: Z. Metallk., 1972, vol. 63, pp. 81-82.

16. M. T. Hepworth, R. P. Smith, and E. T. Turkdogan: Trans. TMS-AIME, 1966, vol. 236, pp. 1278-83.

17. J. H. Swisher and E. T. Turkdogan: Trans. TMS-AIME, 1967, vol. 239, pp. 426-31.

18. G. J. Lloyd and J. W. Martin: Mater. Sci. J., 1972, vol. 6, pp. 7-11.

19. L. S. Darken: Trans. AIME, 1942, vol. 150, pp. 159-69.

20. C. Wagner: Z. Elektrochem., 1959, vol. 63, pp. 772-90.

21. J. H. Swisher and E. O. Fuchs: Trans. TMS-AIME, 1969, vol. 245, pp. 1789-94.

22. J. H. Swisher and E. O. Fuchs: J. Inst. Metals, 1970, vol. 98, pp. 129-33.

23. S. Wood, D. Adamonis, A. Guha, W. A. Soffa and G. H. Meier: ONR Technical Report IO-73-1 on Contract N00014-67-A-402-0008,

24. S. Wood, D. Adamonis, A. Guha, W. A. Soffa, and G. H. Meier: Met. Trans., 1975, vol. 6A, pp. 1793-1800.

25. H. H. Dant, V. Tengler, and G. Häussler: Neue Hütte, 18, 361 (1973).

26. J. Levy and P. Niessen: J. Mater. Sci., 5, 96 (1970).

27. D. H. Howling: Phys. Status Solidi, 18, 579 (1966).

28. M. P. Gupta and H. B. Mathur: Indian J. Chem., 9, 864 (1971).

29. U. Gonser, R. W. Grant, A. H. Muir, Jr., and H. Widersich: Acta Met. 14, 259 (1966).

30. J. Kapteijn: Z. Metallk., 65, 157 (1974).

31. J. L. Meijering: Advances Mat. Res. 5, 1 (1971).

32. P. J. Nolan and P. J. Grundy: J. Mater. Sci. 6, 1143 (1971).

33. G. Böhm and M. Kahlweit: Acta Met., 12, 641 (1964).

34. P. J. Grundy and P. J. Nolan: J. Mater. Sci., 7, 1086 (1972).

35. J. Megusar and G. H. Meier, ONR Technical Report IO-74-2 on Contract N00014-67-A-402-0008, Nov. 1974.

36. J. Megusar and G. H. Meier: Met. Trans., 7A, 1133 (1976).

37. C. E. Wicks and F. E. Block, Thermodynamic Properties of 65 Elements - Their Oxides, Halides, Carbides, and Nitrides, U.S. Bureau of Mines Bulletin 605, (1963).

38. B. Brezny and A. Muan: J. Inorg. Nucl. Chem. 31, 649 (1969).

39. F. Maak: Z. Metallk., 52, 545 (1961).

40. P. Bolsaitis and M. Kahlweit: Acta Met., 15, 765 (1967).

41. I. M. Lifshitz and V. V. Slyozov: J. Phys. Chem. Solids, 19, 35 (1961).

42. C. Wagner: Z. Elektrochem., 65, 581 (1961).

43. G. W. Greenwood, "Particle Coarsening," The Mechanism of Phase Transformations in Crystalline Solids, Monograph and Report Series No. 33 (The Institute of Metals, London, 1969), pp. 103-110.

44. Che-Yu Li and R. A. Oriani, Oxide Dispersion Strengthening, Metallurgical Society Conferences, Vol. 47, Edited by G. S. Ansell, T. D. Cooper and F. V. Lenel (Gordon and Breach, New York, 1968), pp. 431-464.

45. C. Zener: J. Appl. Phys., 20, 950 (1949).

46. A. U. Seybolt, Oxide Dispersion Strengthening, Metallurgical Society Conferences, Vol. 47, Edited by G. S. Ansell, T. D. Cooper and F. V. Lenel (Gordon and Breach, New York, 1968), pp. 469-487.

47. J. A. Dromsky, F. V. Lenel, and G. S. Ansell: Trans. Met. Soc. AIME, 224, 236 (1962).

48. M. H. Lewis, R. H. Seebohm and J. W. Martin, Powder Metallurgy, No. 10 (1962), pp. 87.

49. A. Gatti, Powder Metallurgy, No. 10 (1962), pp. 77.

50. N. Komatsu and N. J. Grant: Trans. Met. Soc. AIME, 230, 1090 (1964).

51. D. M. Williams and G. C. Smith, "A Study of Oxide Particles and Oxide-Matrix Interfaces in Copper," Oxide Dispersion Strengthening, Metallurgical Society Conferences, Vol. 47, Edited by G. S. Ansell, T. D. Cooper and F. V. Lenel (Gordon and Breach, New York, 1968), pp. 509-536.

52. G. R. Woolhouse and L. M. Brown: J. Inst. Metals, 98, 106 (1970).

53. R. G. Faulkner: Scripta Met., 5, 717 (1971).

54. B. Perry and R. E. Smallman: Scripta Met., 6, 149 (1972).

55. H. Fischmeister and E. Navara, Modern Developments in Powder Metallurgy, Ed. by H. H. Hausner, Vol. 5 (Plenum Press, 1971), pp. 97-107.

56. S. K. Bhattacharyya and K. C. Russell: Met. Trans., 3, 2195 (1972).

57. S. K. Bhattacharyya and K. C. Russell: Met. Trans., 7A, 453 (1976).

58. J. Greggi, W. A. Soffa, and G. H. Meier: ONR Technical Report IO-75-3 on Contract N00014-75-C-0747.

59. M. F. Ashby and R. Ebeling: Trans. Met. Soc. AIME, 236, 1396 (1966).

60. A. J. ARdell: Met. Trans., 1, 525 (1970).

61. K. M. Vedula and R. W. Heckel: Met. Trans., 1, 9 (1970).

62. J. Giddings, G. M. Leak, and R. B. Nicholson: Met. Sci., 8, 349 (1974).

63. R. L. Pastorek and R. A. Rapp: Trans. Met. Soc. AIME, 245, 1711 (1969).

64. J. Rexer, Z. Metallk., 63, 745 (1972).

65. R. C. Weast, Handbook of Chemistry and Physics, (49th edition, The Chemical Rubber Co., 18901 Cranwood Pkwy., Cleveland, Ohio 44128, 1968-1969).

66. A. Datta, "Structure and Properties of Copper-Titanium Alloys," (unpublished Ph.D. Dissertation, Department of Metallurgical and Materials Engineering, University of Pittsburgh, 1975).

67. F. E. Rizzo, R. Bidwell, and D. F. Frank: Trans. Met. Soc. AIME, 239, 593 (1967).

68. JANAF Thermochemical Data, Dow Chemical Co., Midland, Mich. (incl. supplements to June 30, 1970).

69. R. E. Ebeling and M. F. Ashby: Phil. Mag., 13, 805 (1966).

70. P. B. Hirsch and F. J. Humphreys: Proc. Royal Soc. London, 318A, 45 (1970).

LIST OF FIGURES

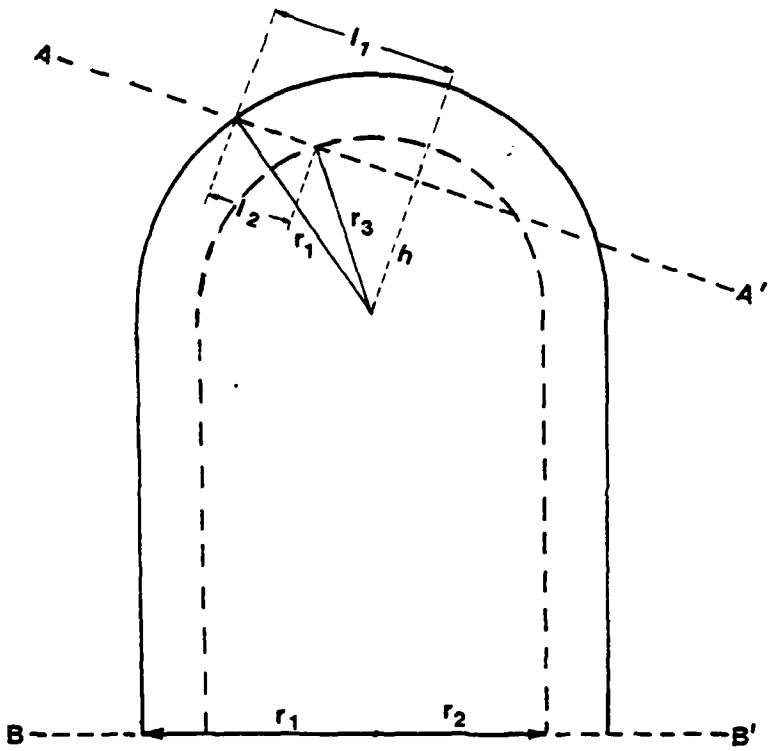

Figure 1. Sectioning Method for Spherical and Cylindrical Geometries.

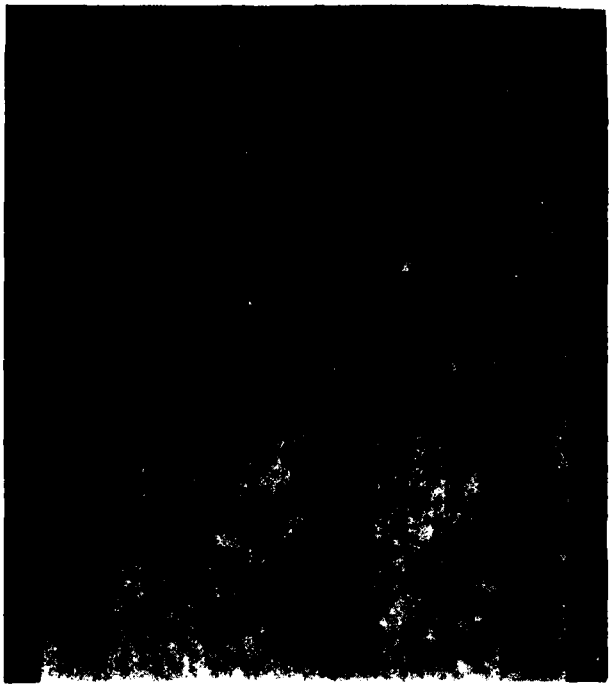

Figure 2. Cu-0.29 wt pct Ti Alloy, Internally Oxidized 20 hr. at 900°C, 12X.

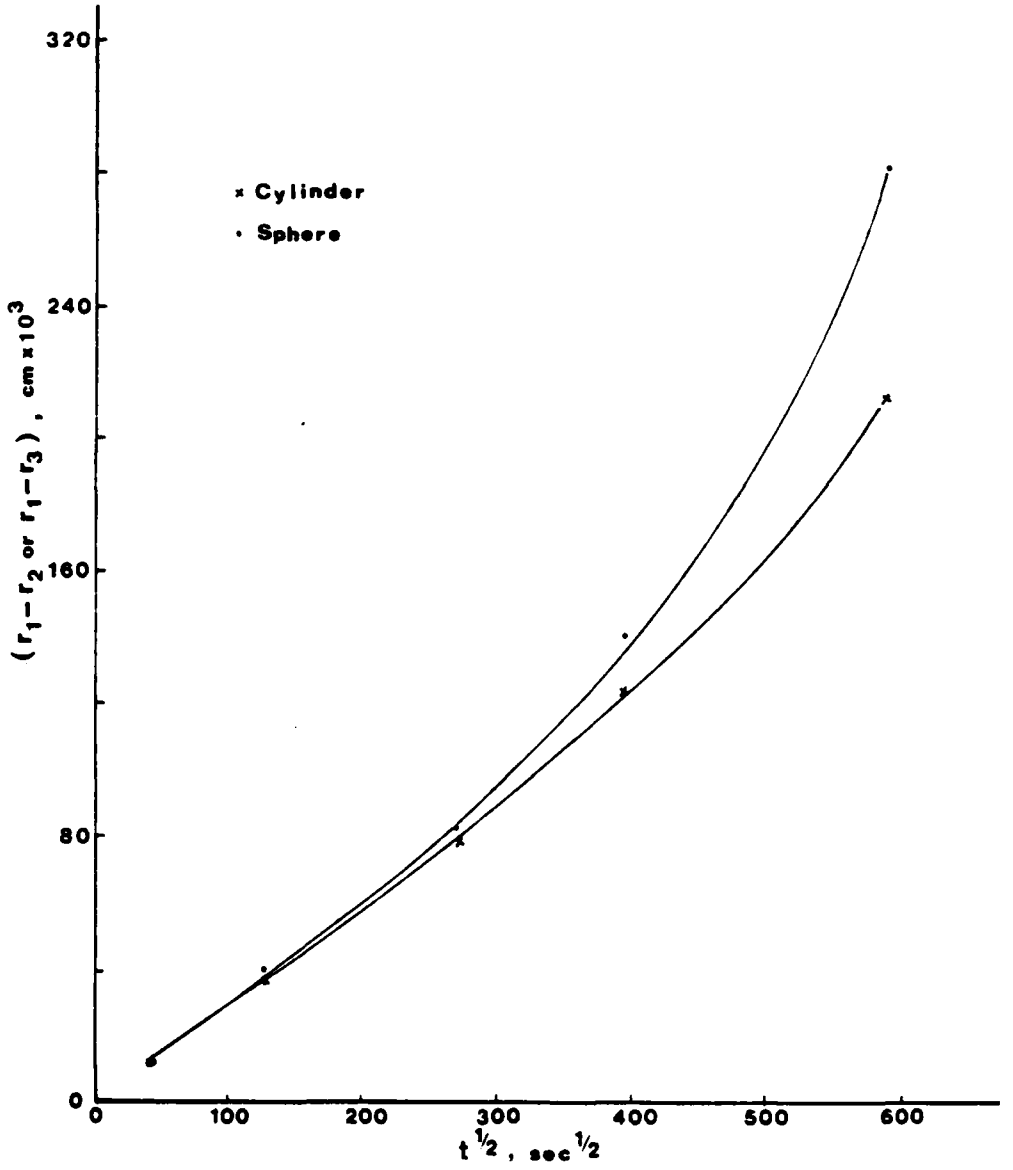

Figure 3. Internal oxidation penetration as a function of time at 900°C.

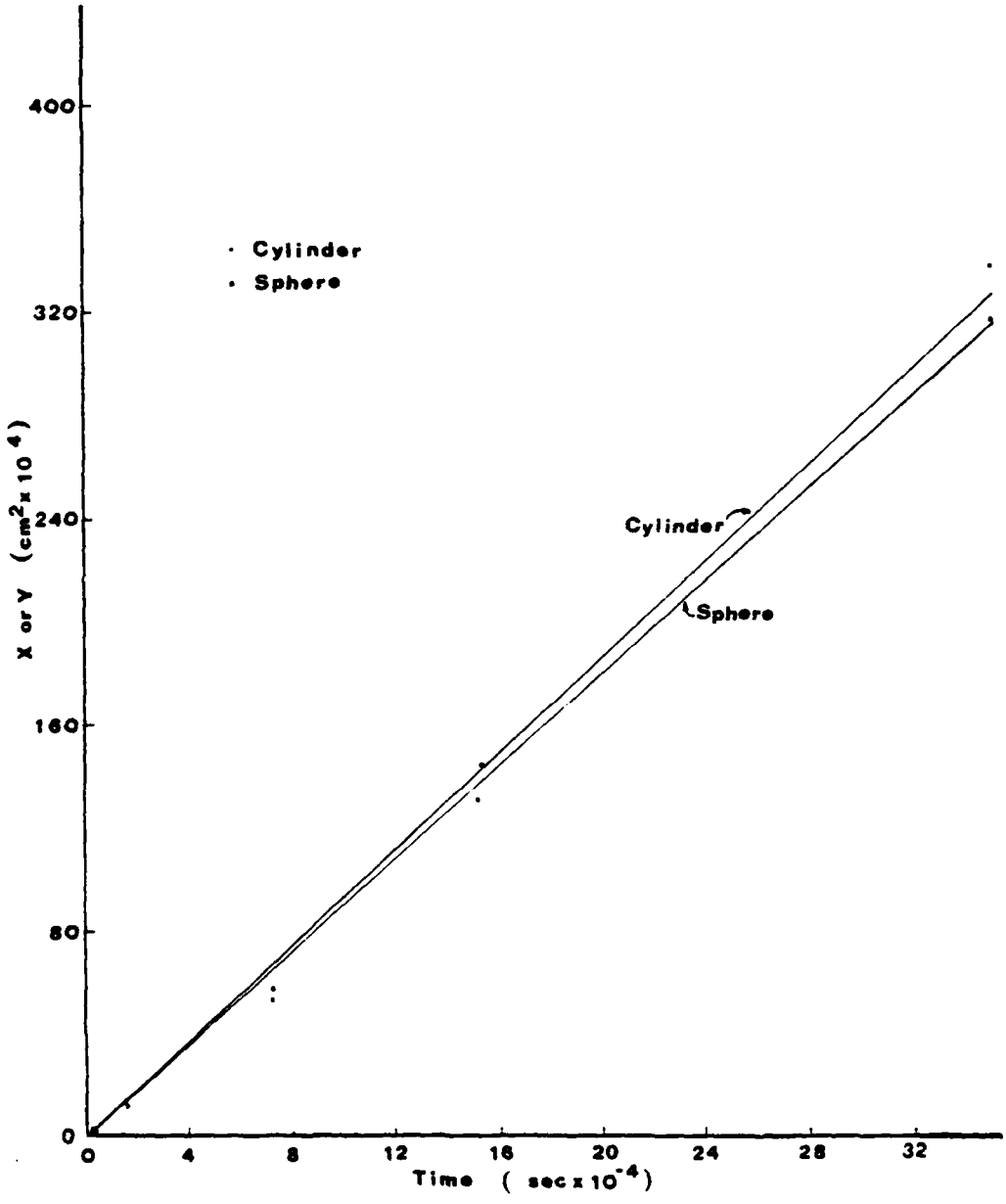

Figure 4. Penetration Parameter X or Y vs time at 900°C.

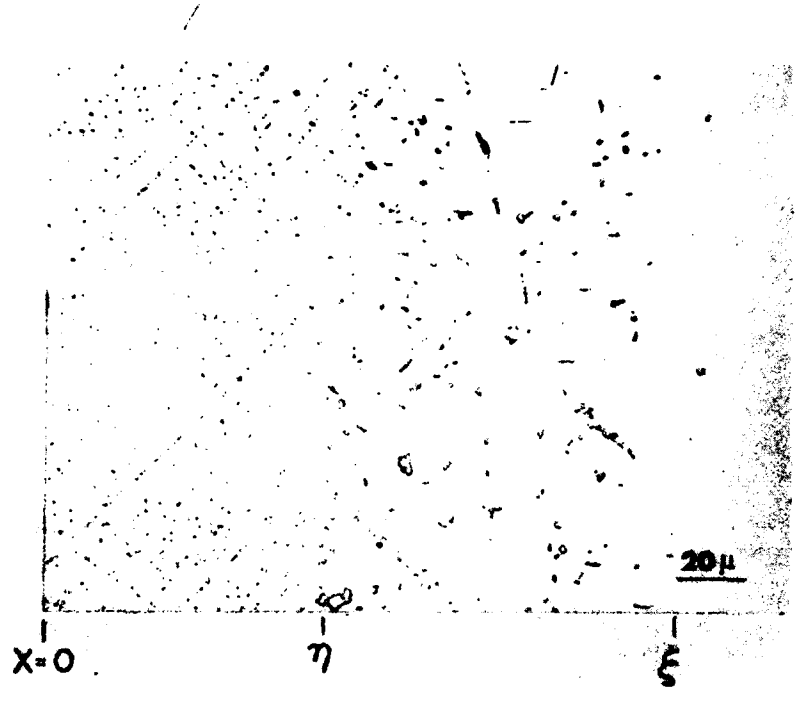

Figure 5. Co-0.5 wt% Ti Alloy Internally Oxidized for 528 Hours at 900°C. Unetched. Magnification: 500X.

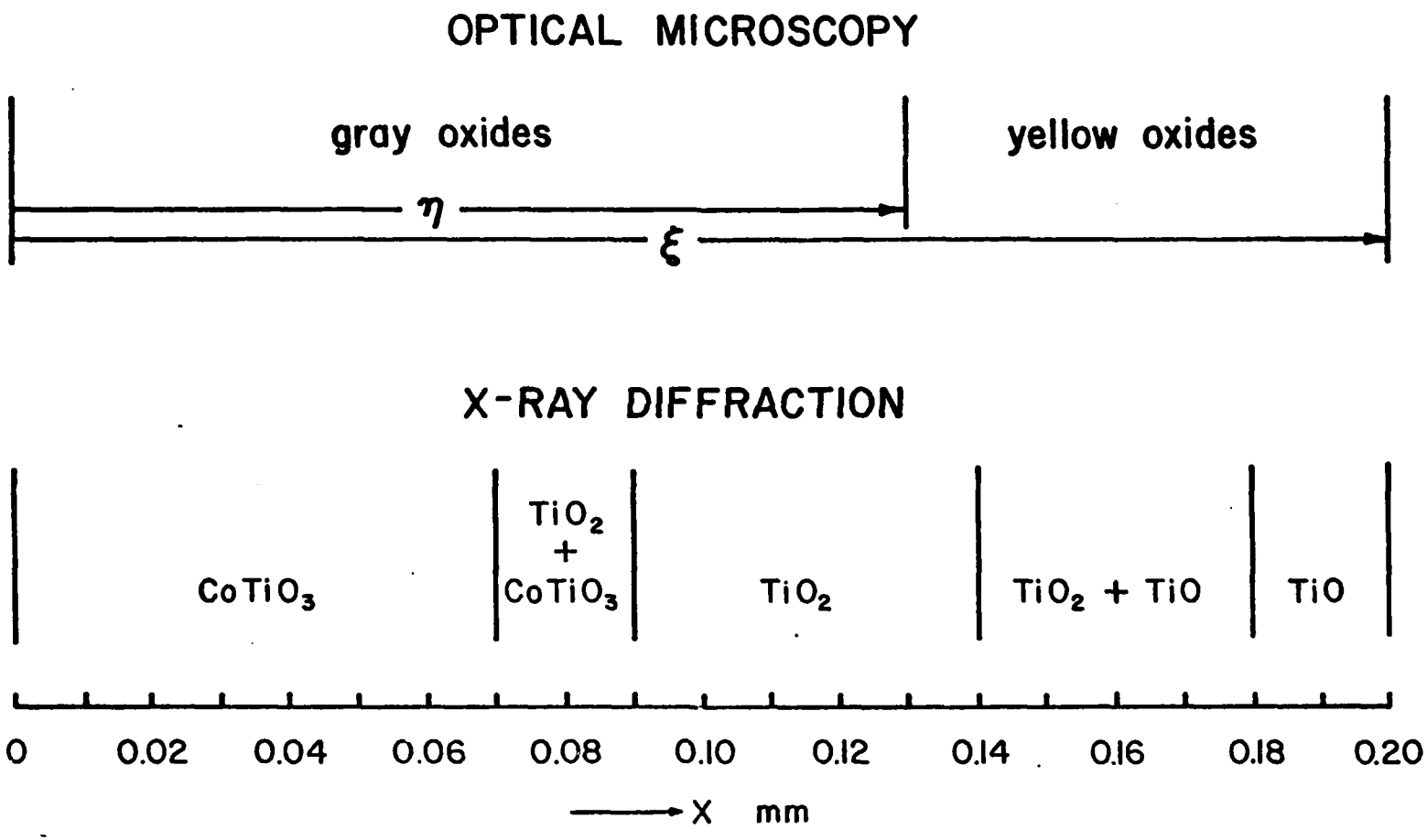

Figure 6. Morphology and Structure of Oxide Particles as a Function of Penetration Depth in Co-3.01 wt% Ti Alloy Internally Oxidized at 1080°C.

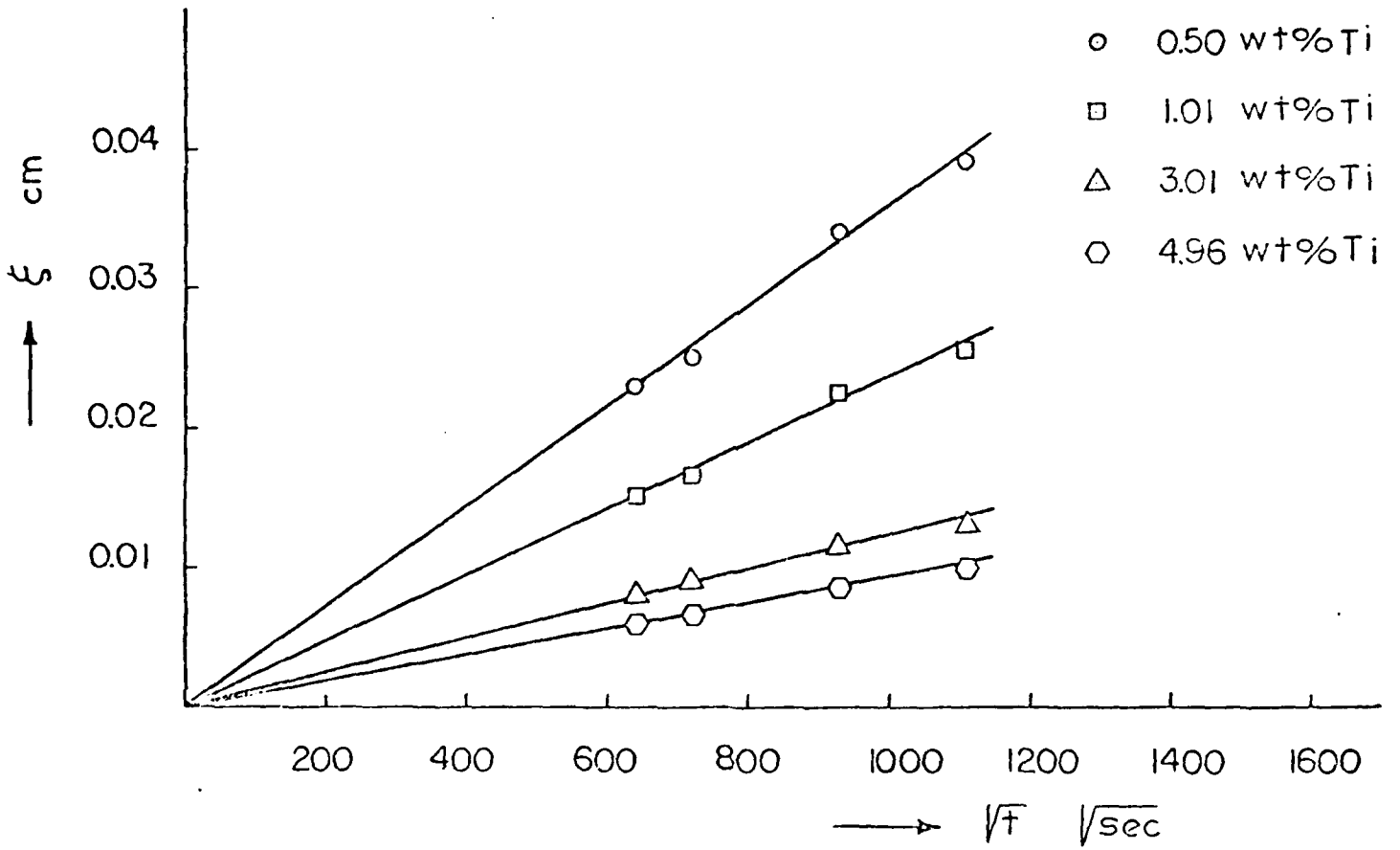

Figure 7. Plot of Penetration Depth ξ of Internal Oxidation Zone Versus Square Root of Time, t, for Four Co-Ti Alloys Internally Oxidized at 1000°C.

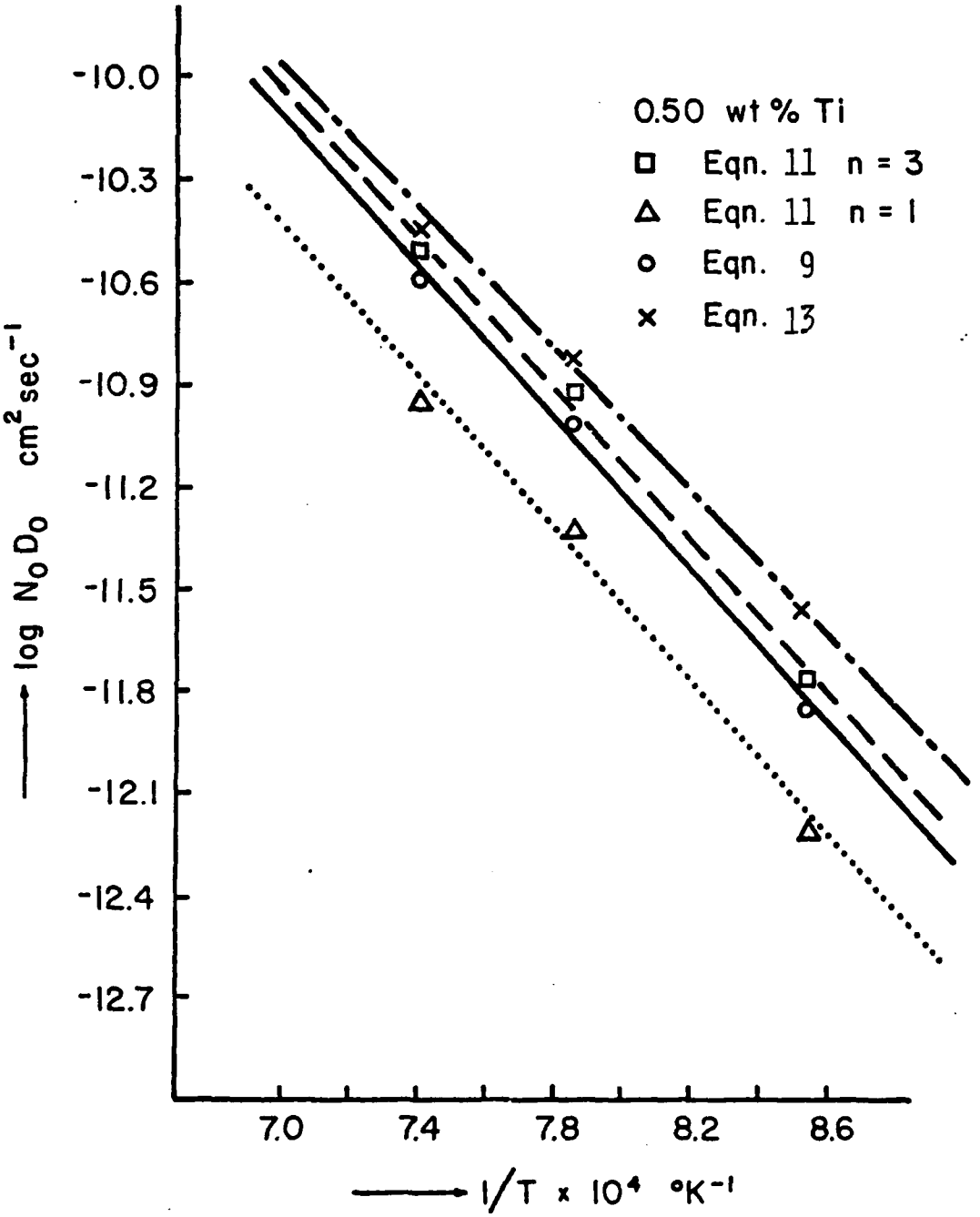

Figure 8. Plot of Logarithm of N_0D_0 Versus Reciprocal Temperature, 1/T, For Co-0.50 wt% Ti Alloy.

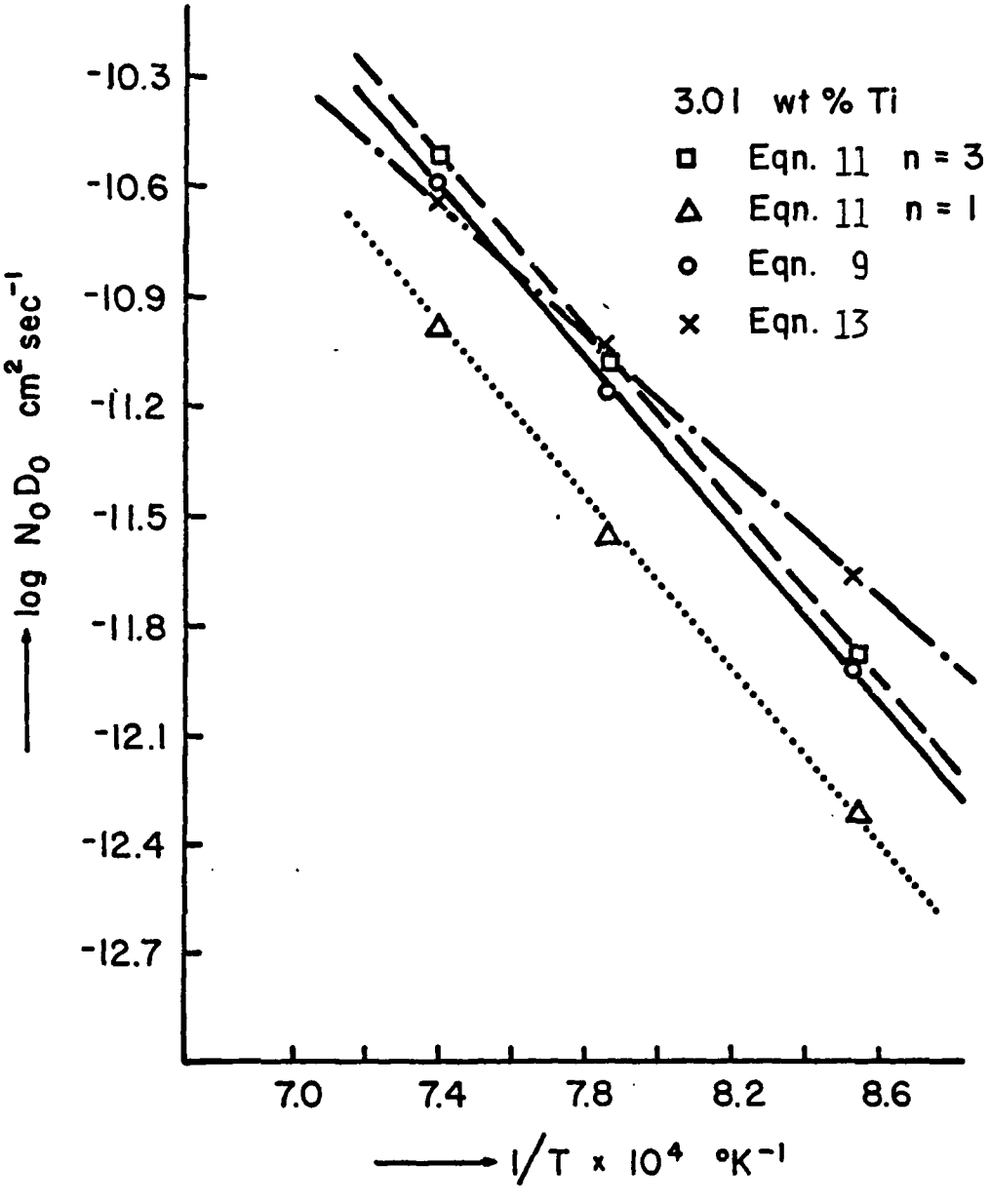

Figure 9. Plot of Logarithm of N_0D_0 Versus Reciprocal Temperature, 1/T, For Co-3.01 wt% Ti Alloy.

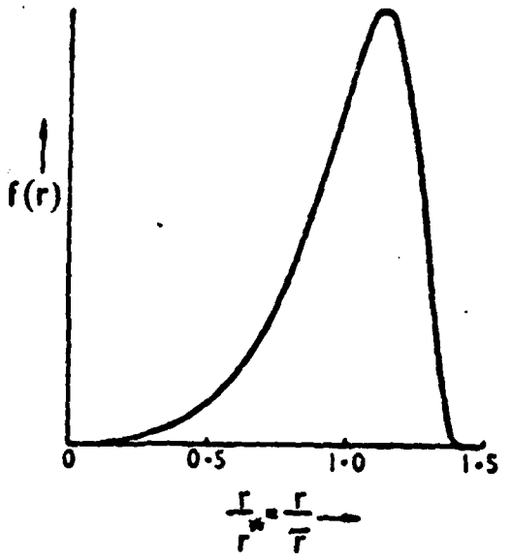

(a)

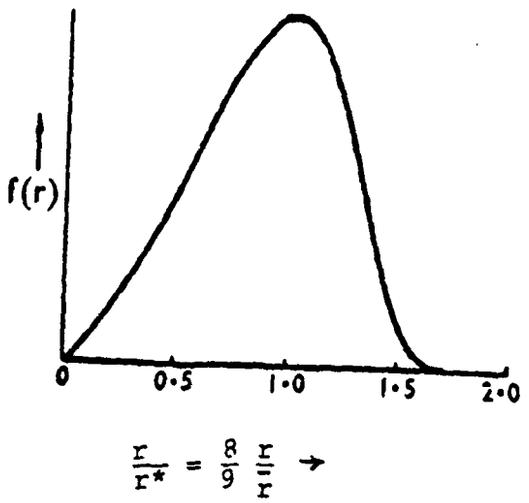

(b)

Figure 10(a). Particle size distribution predicted after long periods of time under conditions of diffusion-controlled coarsening plotted from equation (24).

Figure 10(b). Particle size distribution predicted after a long period of interface-controlled coarsening, plotted from equation (29).

Figure 11. Carbon extraction replica showing TiO_2 particles, coarsened in vacuum for 101 hrs at 904°C; $\bar{d}$ = 91.5 Å.

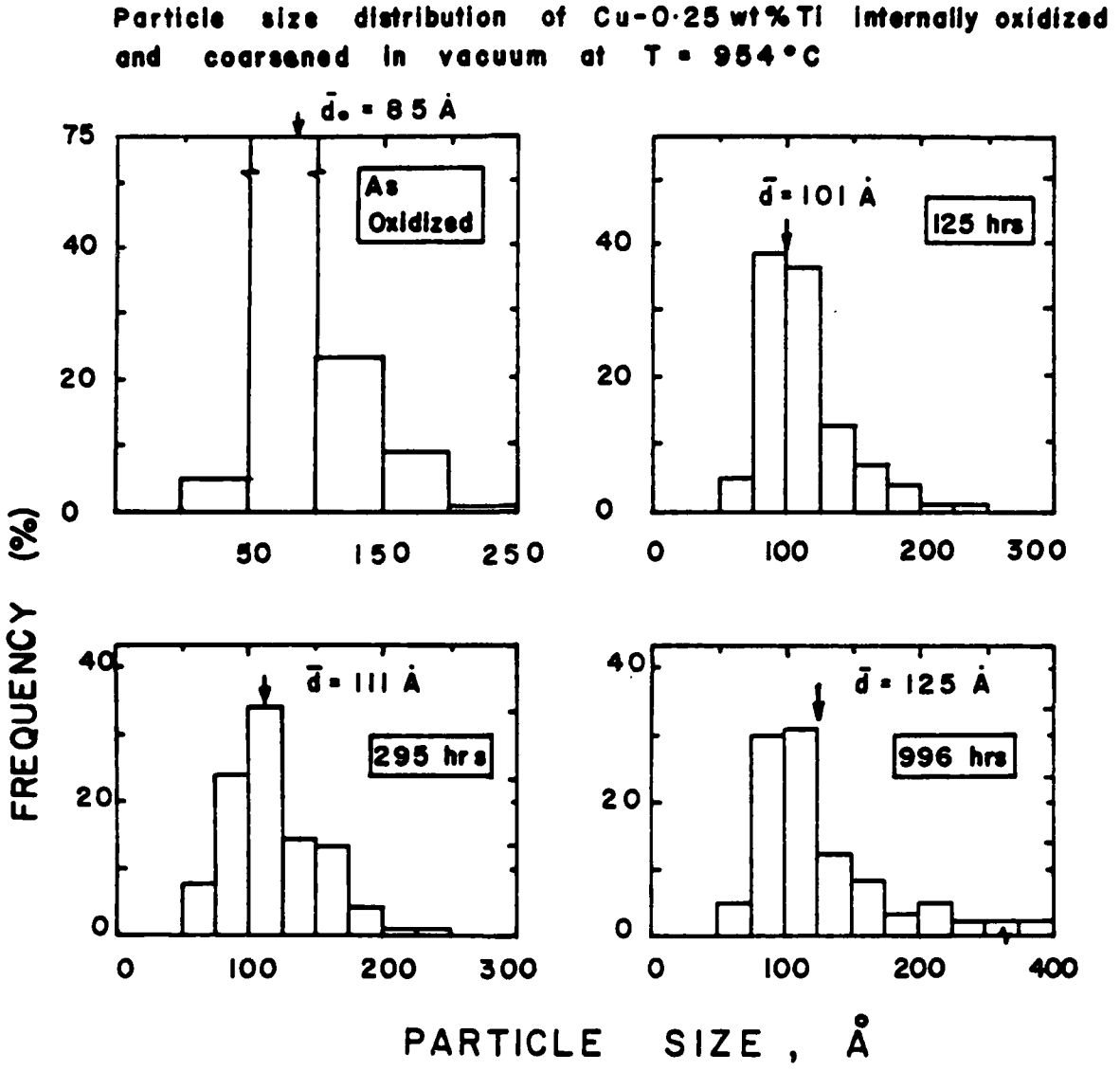

Figure 12. Particle size distribution of Cu-0.25 wt pct Ti internally oxidized and coarsened in vacuum at T = 954°C.

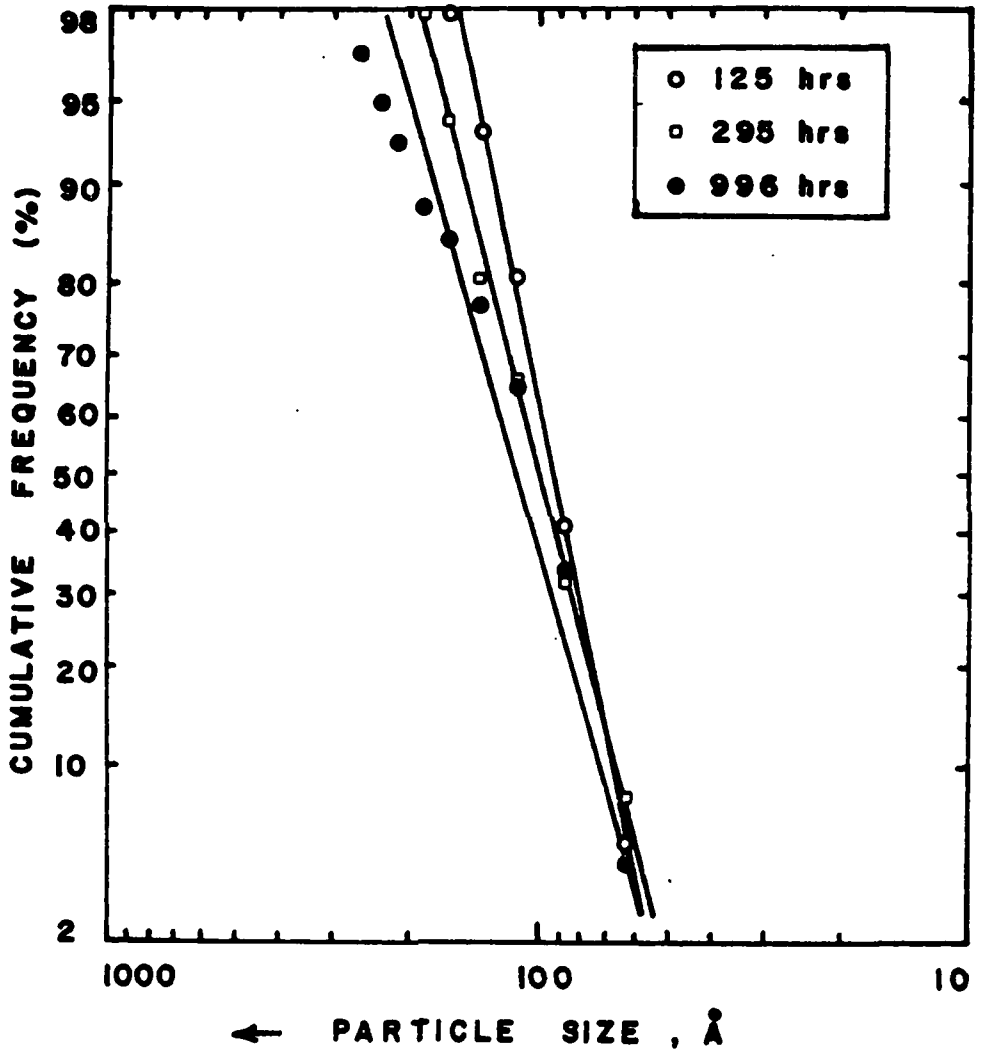

Figure 13. Log-normal probability plots for particle size distribution of Cu-0.25 wt pct Ti internally oxidized and coarsened in vacuum at T = 954°C.

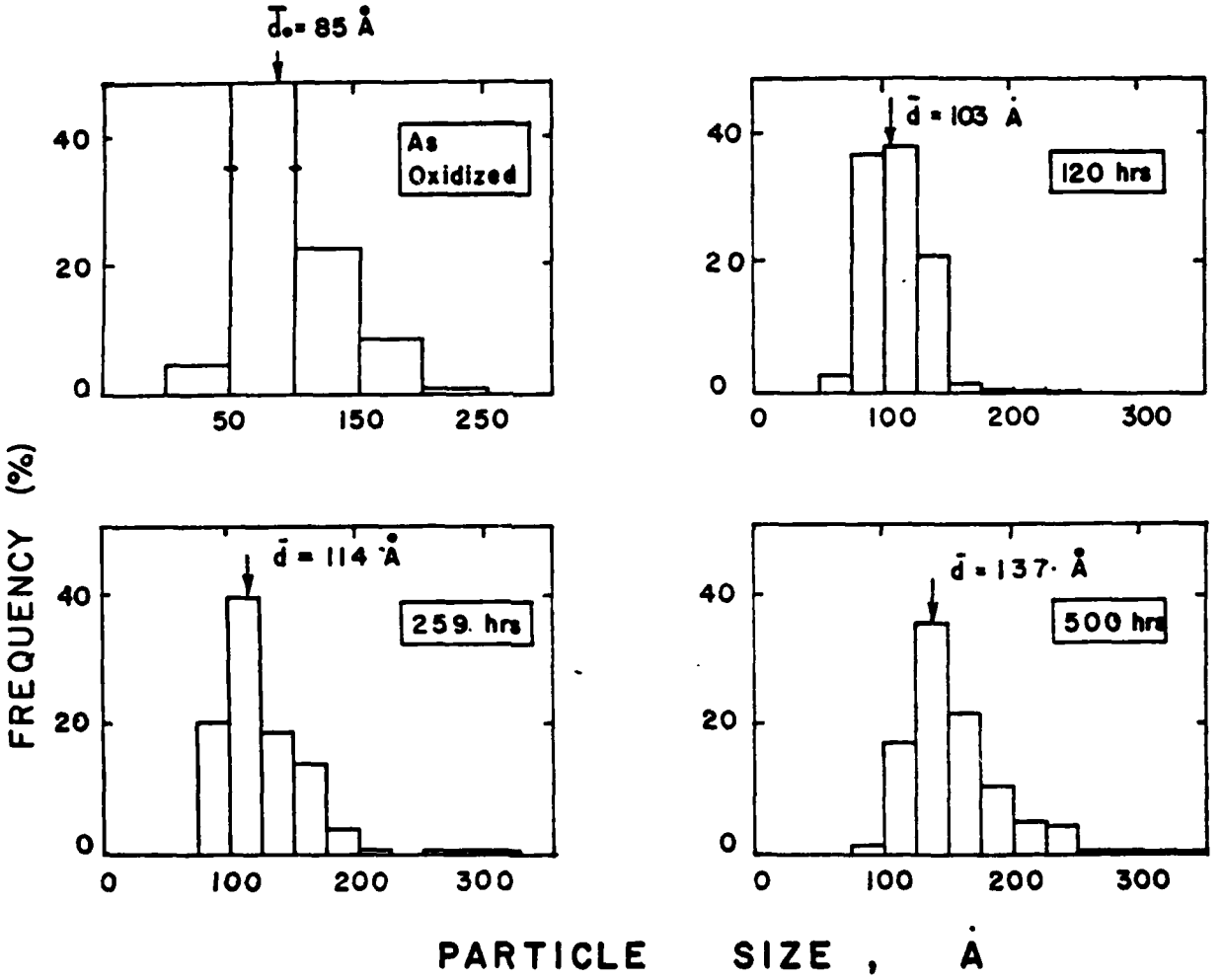

Figure 14. Particle size distribution of Cu-0.25 wt pct Ti internally oxidized and coarsened in Cu/Cu_2O at T = 951°C.

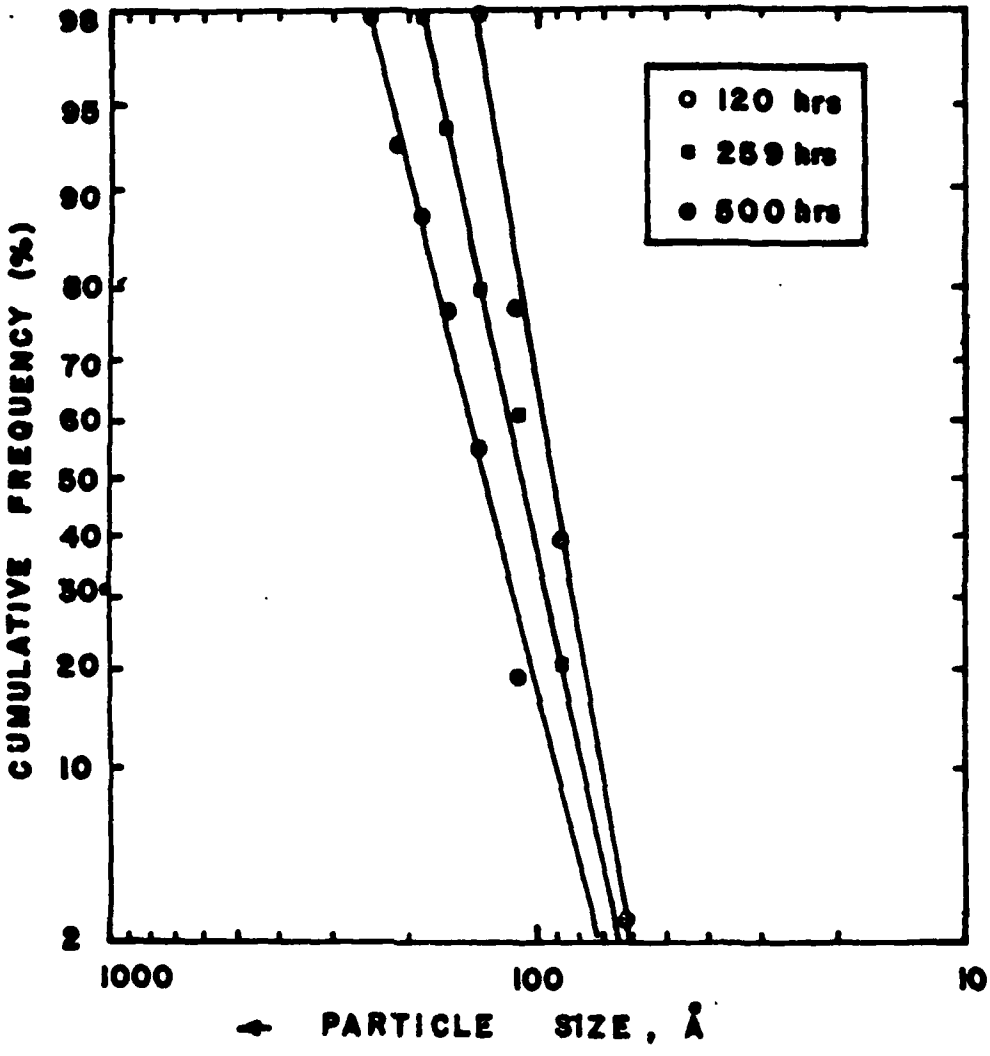

Figure 15. Log-normal probability plots for particle size distribution of Cu-0.25 wt pct Ti internally oxidized and coarsened in Cu/Cu_2O at T = 951°C.

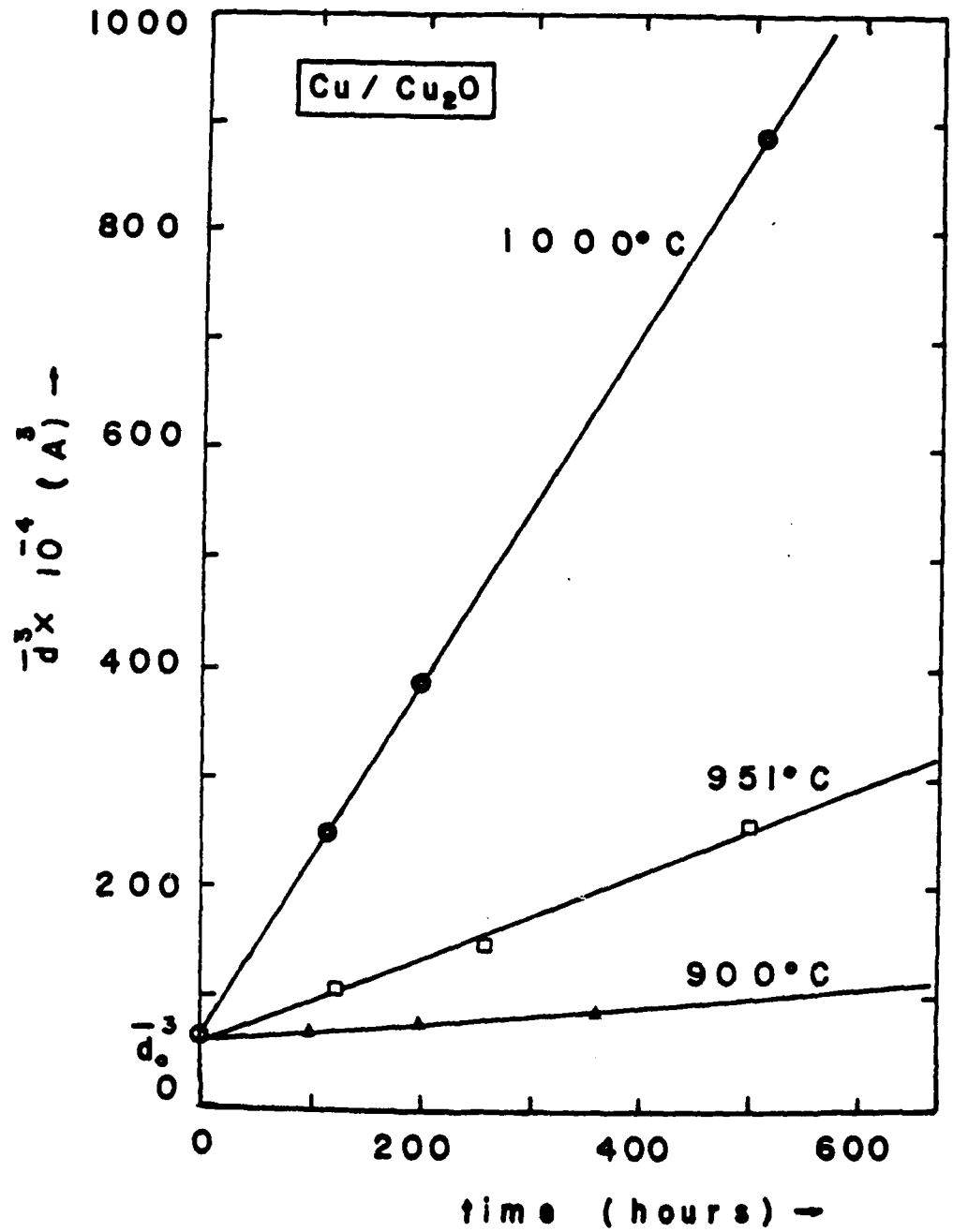

Figure 16. Variation of average particle size cubed as a function of time for TiO_2 oxide particles coarsened in Cu/Cu_2O.

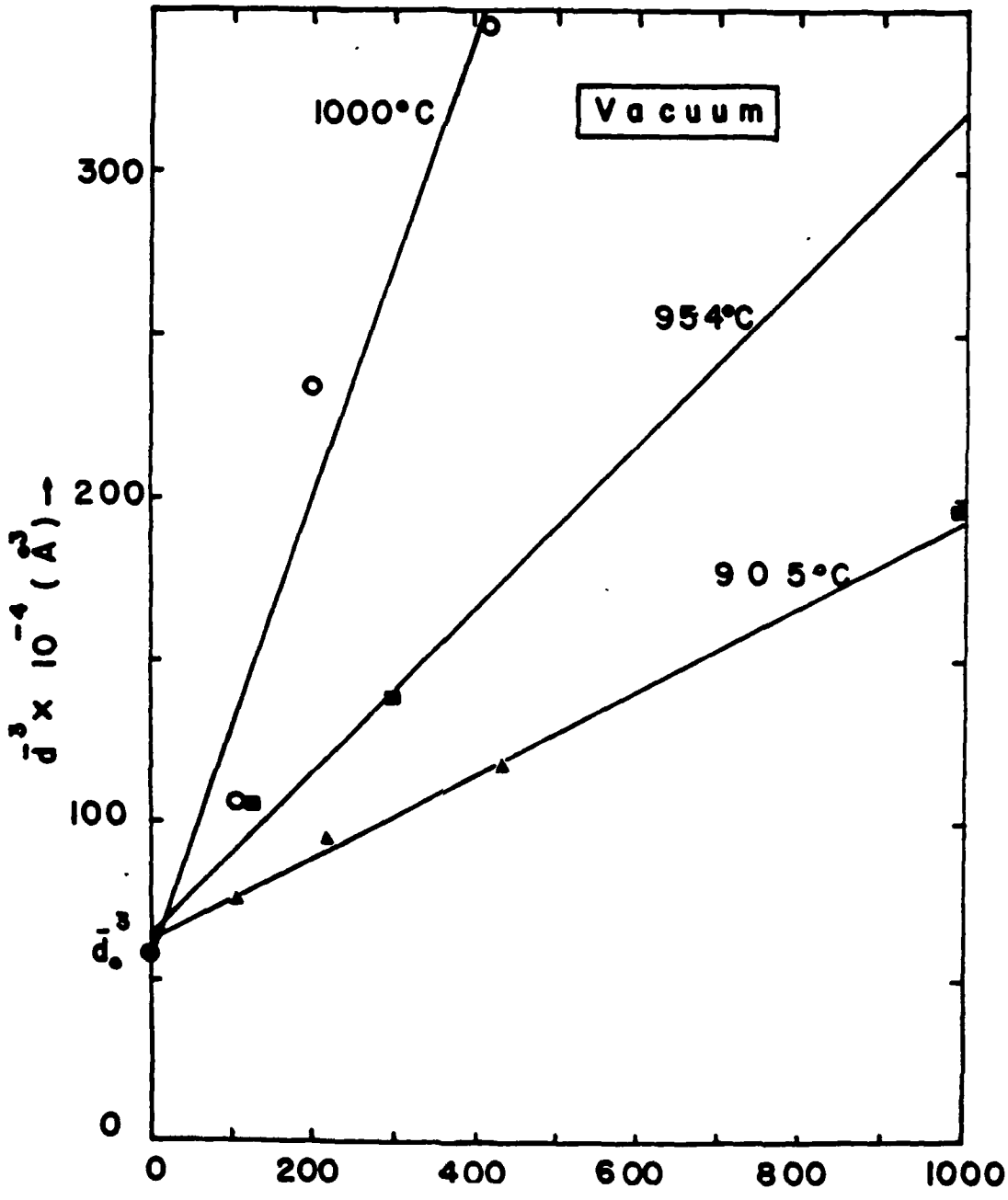

Figure 17. Variation of average particle size cubed as a function of time for TiO_2 oxide particles coarsened in vacuum.

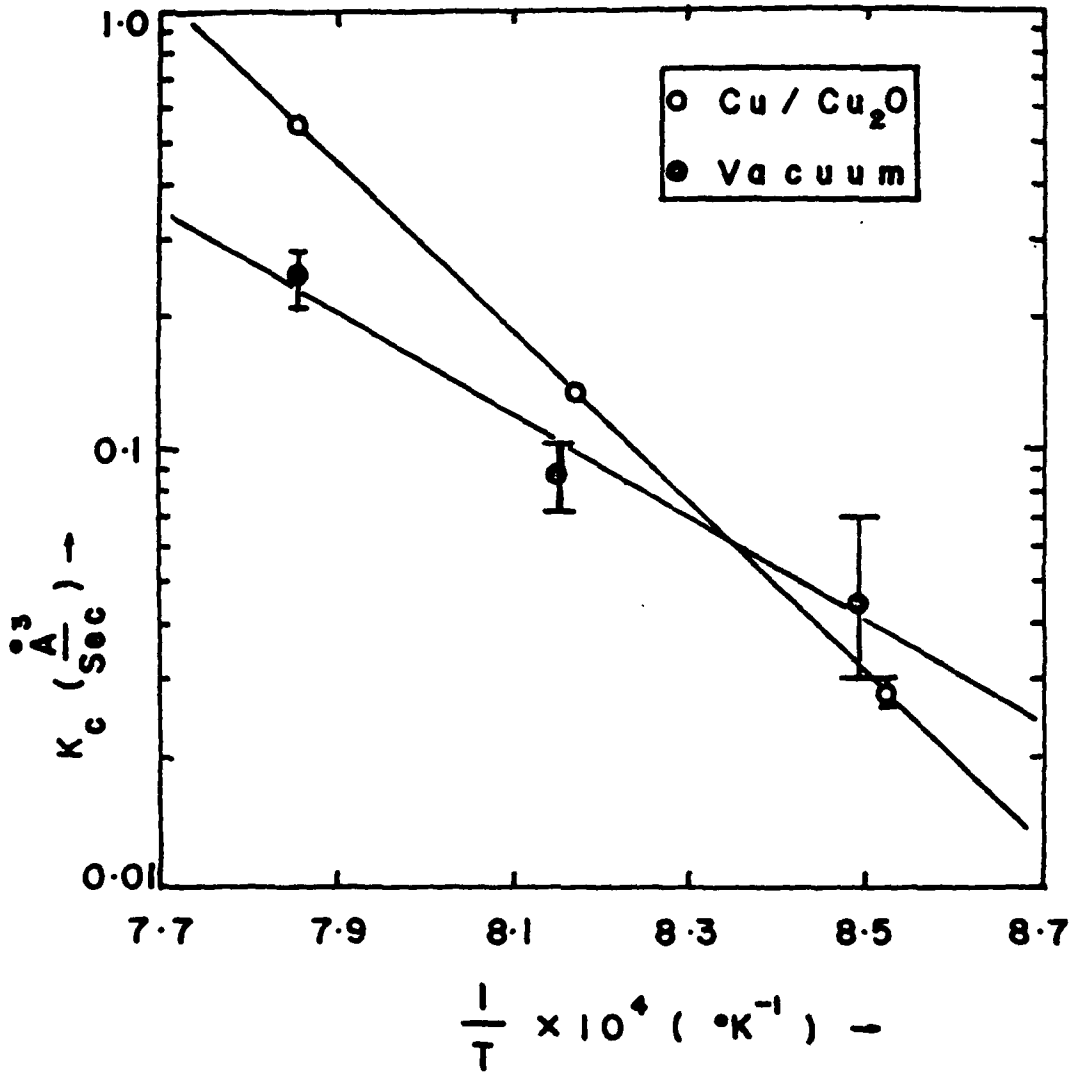

Figure 18. Arrhenius plot of the coarsening rate constants in a Cu-0.25 wt pct Ti alloy coarsened in vacuum and Cu/Cu_2O.

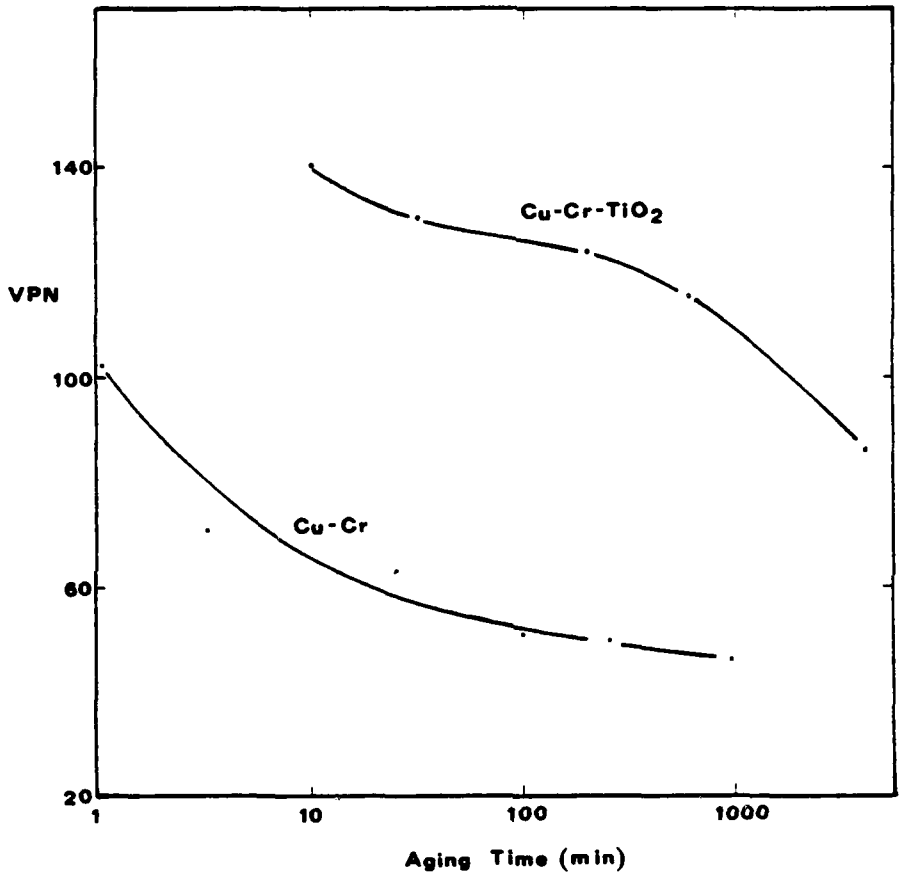

Figure 19. Aging Curves for Cu-0.2 Cr and Cu-0.2 Cr-TiO_2 Alloys at 700°C.

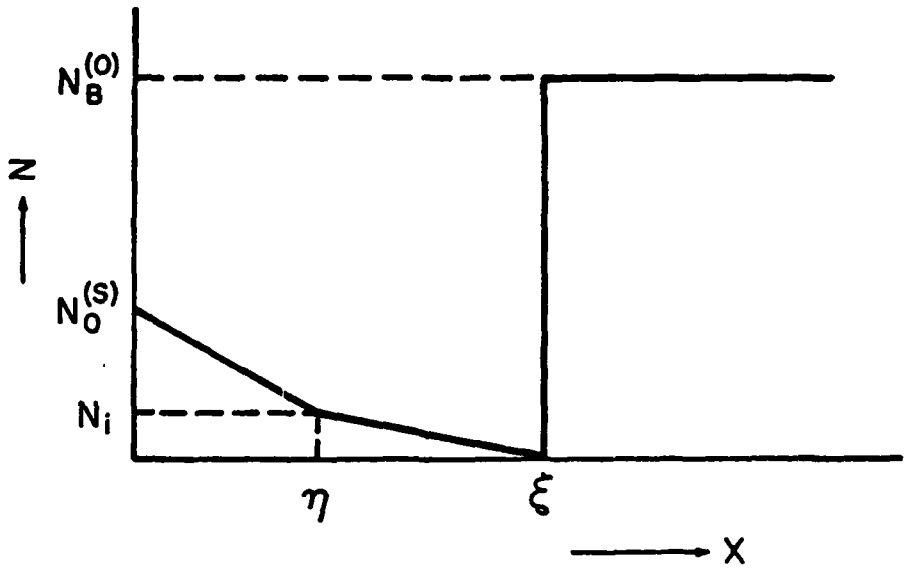

Figure 20. Concentration of Oxygen N_O and Solute N_B as a Function of Distance x (Ref. 31).

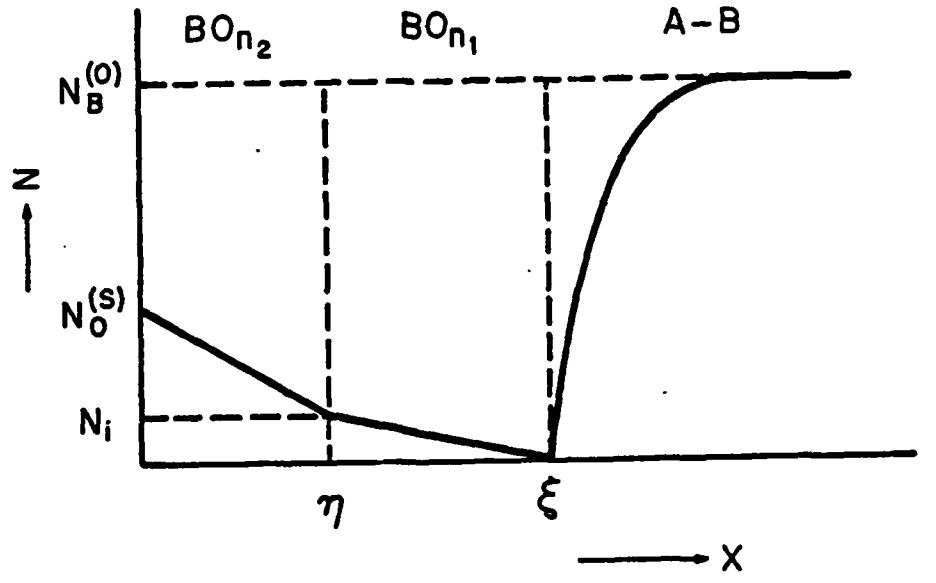

Figure 21. Concentration of Oxygen N_O and Solute N_B as a Function of Distance x when Solute Counterdiffusion is Significant.

LIST OF TABLES

Table 1 Solubility-Diffusivity Products
for Oxygen in Copper Cu-29 wt% Ti

Temp. °C	$N_O^{(s)} D_O$ calculated from spherical part cm^2/cm	$N_O^{(s)} D_O$ calculated from cylindrical part $cm^2 sec$
700	1.36×10^{-12}	1.34×10^{-12}
750	1.11×10^{-11}	1.02×10^{-11}
800	5.39×10^{-11}	4.67×10^{-11}
850	1.16×10^{-10}	1.13×10^{-10}
900	3.50×10^{-10}	3.67×10^{-10}

Temperature (°C)	Time (sec $^{1}/_{2}$)	f = η/ξ		
		N_{Ti}=0.0061	N_{Ti}=0.0124	N_{Ti}=0.0370
900	1610	----	----	----
	1500	0.44	0.47	0.52
	1380	0.41	0.46	0.52
	1250	0.43	0.45	0.54
1000	1100	0.49	0.56	0.66
	930	0.50	0.54	0.63
	720	0.53	0.61	0.69
	630	0.54	0.58	0.67
1080	720	0.56	0.61	0.71
	588	0.58	0.62	0.71
	510	0.57	0.63	0.70
	417	0.58	0.61	0.71

Table 2 Measured Values of Parameter f as a Function of Titanium Content, N_{Ti}, and Time at Oxidation Temperatures 900°, 1000° and 1080°C.

Temperature (°C)	N_{Ti}	m	f	n_{eff}	ξ^2/t ($cm^2/sec \times 10^{10}$)	$N_O^{(s)} D_O$ (cm^2/sec)
	0.0061	0.26	0.68	2.46	34.0	$2.55 \times 10^{-11} \pm 5.7 \times 10^{-12}$
1080	0.0124	0.26	0.68	2.46	15.1	$2.30 \times 10^{-11} \pm 5.8 \times 10^{-12}$
	0.0370	0.26	0.68	2.46	5.57	$2.54 \times 10^{-11} \pm 5.4 \times 10^{-12}$
	0.0061	0.23	0.71	2.52	12.57	$9.84 \times 10^{-11} \pm 7.9 \times 10^{-13}$
1000	0.0124	0.23	0.71	2.52	5.59	$8.73 \times 10^{-12} \pm 7.9 \times 10^{-13}$
	0.0370	0.23	0.71	2.52	1.46	$6.81 \times 10^{-12} \pm 5.0 \times 10^{-14}$
	0.0061	0.19	0.75	2.53	1.78	$1.37 \times 10^{-12} \pm 4.5 \times 10^{-13}$
900	0.0124	0.19	0.76	2.53	0.83	$1.30 \times 10^{-12} \pm 4.5 \times 10^{-13}$
	0.0370	0.19	0.76	2.53	0.26	$1.22 \times 10^{-12} \pm 1.9 \times 10^{-13}$

Table 3 Calculation of Solubility-Diffusivity Product $N_O D_O$ by Assuming that Both TiO_2 (n_1=2) and $CoTiO_3$ (n_2=3) are Present and Using Meijering Analysis.

Table 4 Solubility Diffusivity Products for Oxygen in Cobalt Calculated from Equation 13

$T(^{o}C)$	$N_{Ti}^{(o)}$	$N_O^{(s)} D_O (cm^2/sec)$
900	0.0061	$2.9 \times 10^{-12} \pm 2.7 \times 10^{-13}$
900	0.0124	$2.7 \times 10^{-12} \pm 2.0 \times 10^{-13}$
900	0.0370	$2.3 \times 10^{-12} \pm 2.5 \times 10^{-13}$
1000	0.0061	$1.6 \times 10^{-11} \pm 1.1 \times 10^{-12}$
1000	0.0124	$1.3 \times 10^{-11} \pm 1.6 \times 10^{-12}$
1000	0.0370	$8.6 \times 10^{-12} \pm 6.4 \times 10^{-13}$
1080	0.0061	$3.5 \times 10^{-11} \pm 1.7 \times 10^{-12}$
1080	0.0124	$3.0 \times 10^{-11} \pm 2.6 \times 10^{-12}$
1080	0.0370	$2.4 \times 10^{-11} \pm 1.7 \times 10^{-12}$

Table 5

Effect of Atmosphere on the Coarsening Rate and the Activation Energy of Coarsening of TiO_2 Dispersions in Cu

A. Vacuum Atmosphere

Temperature ^{o}C	905	954	1000
Coarsening Rate, $\frac{A^3}{sec}$	0.04	0.08	0.25
Activation Energy	$53 \pm 8 \frac{Kcal}{mole}$		

B. Cu/Cu_2O Atmosphere

Temperature ^{o}C	900	951	1000
Coarsening Rate, $\frac{A^3}{sec}$	0.02	0.13	0.56
Activation Energy	$89.4 \pm 0.3 \frac{Kcal}{mole}$		

Table 6 Summary of Mechanical Properties

Temp °C	Initial Yield Kg/mm^2	0.2% Yield Kg/mm^2	UTS Kg/mm^2	% Elongation
		Cu-0.24 wt pct Ti		
750	15.7	16.6	28.0	23
800	14.5	15.5	27.0	24
850	14.2	14.5	25.6	23
900	13.1	13.8	24.7	26
		Cu-0.47 wt pct Ti		
800	20.1	20.7	28.7	16
850	18.2	19.4	29.2	24.9
900	18.0	18.8	24.7	27
		Cu-0.98 wt pct Ti		
850	24.8	25.7	33.0	14
900	23.4	24.5	32.4	15
950	21.8	23.3	32.1	20
1000	16.9	18.1	28.5	13